SERI/STR-211-3114
DE87001145

February 1987

Photochemical Vapor Deposition of Amorphous Silicon Photovoltaic Devices

Annual Subcontract Report 1 May 1985 - 30 April 1986

B. N. Baron
R. E. Rocheleau
S. S. Hegedus
Institute of Energy Conversion
University of Delaware
Newark, Delaware

Prepared under Subcontract No. XB-4-04061-1

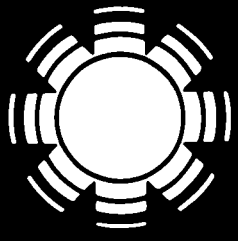

SERI

Solar Energy Research Institute
A Division of Midwest Research Institute

1617 Cole Boulevard
Golden, Colorado 80401-3393

Operated for the
U.S. Department of Energy
under Contract No. DE-AC02-83CH10093

Printed in the United States of America
Available from:
National Technical Information Service
U.S. Department of Commerce
5285 Port Royal Road
Springfield, VA 22161

Price: Microfiche A01
Printed Copy A04

Codes are used for pricing all publications. The code is determined by the number of pages in the publication. Information pertaining to the pricing codes can be found in the current issue of the following publications, which are generally available in most libraries: *Energy Research Abstracts, (ERA); Government Reports Announcements* and Index (*GRA* and I); *Scientific and Technical Abstract Reports (STAR);* and publication. NTIS-PR-360 available from NTIS at the above address.

SERI/STR-211-3114
UC Category: 63
DE87001145

SERI/STR--211-3114
DE87 001145

Photochemical Vapor Deposition of Amorphous Silicon Photovoltaic Devices

Annual Subcontract Report
1 May 1985 - 30 April 1986

B. N. Baron
R. E. Rocheleau
S. S. Hegedus
Institute of Energy Conversion
University of Delaware
Newark, Delaware

February 1987

SERI Technical Monitor: B. Stafford

Prepared under Subcontract No. XB-4-04061-1

Solar Energy Research Institute
A Division of Midwest Research Institute

1617 Cole Boulevard
Golden, Colorado 80401-3393

Prepared for the
U.S. Department of Energy
Contract No. DE-AC02-83CH10093

TABLE OF CONTENTS

LIST OF FIGURES

LIST OF TABLES

PREFACE

This report describes the first twelve months of research directed to studies of photochemical vapor deposition for fabricating amorphous silicon based thin-film solar cells. The University of Delaware invested significant resources in the laboratory facilities and equipment needed to perform the research. The interest and support shown by the Solar Energy Research Institute, Solar Electric Division deserve special recognition. Collaboration between this program and work being carried out under SERI Subcontract XL-5-04074-3 has proven to be invaluable.

The following personnel at the Institute of Energy Conversion have contributed to the work described in this report:

Program Manager	B. N. Baron
Principal Investigator	R. E. Rocheleau
Reactor Design/Construction	S. C. Jackson W. A. Buchanan P. Wilson R. Dozier S. Beard
Film Deposition	W. A. Buchanan
Material Characterization	S. S. Hegedus A. R. Moore R. Dozier G. Streetman
Device Fabrication	L. C. DiNetta J. A. Hall A. Canedo
Device Analysis	S. S. Hegedus S. Buchanan

SUMMARY

Objective:

The objective of this research program is to fabricate efficient, stable, single junction amorphous silicon:hydrogen p-i-n solar cells by ultraviolet photo-dissociation of disilane at growth rates exceeding 0.1nm/sec. The primary goal of the research to date was to fabricate 7% p-i-n solar cells by photo-CVD.

Discussion:

Ultraviolet photolysis of mercury-sensitized disilane was selected for depositing a-Si:H films for materials characterization and device development. Several reactor designs were evaluated with primary emphasis on avoiding window fouling. A novel reactor was designed and constructed. The reactor includes a UV transparent moveable Teflon curtain to minimize deposition on the reactor window. UV light is provided by a low pressure mercury grid lamp. Two reactor systems were built. The design and construction of the reactor systems included provisions for safe handling of toxic and flammable gases.

Depositions of undoped a-Si:H were carried out over a range of deposition conditions using both silane and disilane diluted in He. Other reactor conditions included: flow rates, 10-20 sccm; reactor pressure, 5-15 torr; mercury partial pressure, less than 0.01 to 0.034 torr; substrate temperature, 200-280°C. Undoped films were deposited at rates up to 0.10 nm/sec on a variety of substrates for characterization of electrical and optical properties. A systematic study of the influence of substrate temperatures yielded intrinsic a-Si:H films deposited at 240°C having bandgap = 1.85 eV, σ_p = 2.5 x10^{-9} S/cm, σ_p/σ_d= 2x10^{3} and E_A = 0.64eV.

Doped, n- and p-type, a-Si:H films were deposited by photolysis of Hg-sensitized silane and disilane. P-type a-Si:H films with E_A = 0.4eV and σ_d up to 5x10^{-5} S/cm were obtained by adding 0.5-3.0 vol % B_2H_6 to the silane or disilane. P-type a-SiC:H films were deposited with 10 to 40% methylsilane in silane. The best films of this type for cells had a dark conductivity of 1X10^{-9} S/cm and E_A=0.38eV at a bandgap of 1.9eV. N-type films with E_a = 0.25eV were obtained by adding 1-2 vol % PH_3.

Devices with the configuration glass/TCO/p-i-n/metal were fabricated using photo-CVD a-Si:H layers. Cell areas of 0.09 cm^2 were defined using photo-lithography. Cell testing was performed with 87.5 mW/cm^2, ELH illumination. The highest cell efficiency was achieved with an Ag/Mg/Al contact and a 300nm thick i-layer. Following 1 hour of heat treatment at 150°C in air, the cell efficiency was 6.44% with: V_{oc}=.644V, J_{sc}=12.9 mA/cm^2, and

FF=67.9%. Voltage bias had little effect on the quantum efficiency from 400 to 700 nm. This together with the relatively high FF indicates negligible collection losses due to electron-hole recombination. The open circuit voltage which is lower than expected from the measured film properties, may be limited by impurities or insufficient doping of the thin p- and n-layers or by poor p/i interfaces such as due to boron tailing.
Future work will include optimizing doped layer conductivity, reducing residual gases, especially $H_{2}O$ in the reactor, optimizing i-layer thickness and properties, enhancing i-layer deposition rate and characterizing photo-CVD reactor kinetics.

Summary:

- A novel photo-CVD reactor which minimizes window fouling was designed and constructed.

- Intrinsic a-Si:H films were deposited and characterized.

- N-type and p-type a-Si:H and p-type a-SiC:H films were deposited and characterized.

- A glass/TCO/p-i-n/metal photovoltaic cell with 6.4% efficiency (87.5 mW/cm^{2},ELH) was fabricated by photo-CVD.

SECTION 1.0

INTRODUCTION

Chemical vapor deposition techniques, in particular plasma enhanced CVD, have been used to produce high efficiency a-Si:H p-i-n devices. Several research groups have reported devices with over 10% efficiencies using the plasma enhanced CVD (glow discharge) technique. Further development of a-Si:H devices to the point where they will make a contribution to U.S. electrical energy production requires additional research directed to increased efficiency, improved photo-stability, and translation of scale to commercial production.

Research on alternate deposition techniques(1) is likely to lead to improved understanding of the relationships between deposition processes and material properties. Technical options for achieving the properties needed for higher efficiency and long term stability can be expected from such research. Furthermore, understanding of the fundamental chemical processes which govern film growth are required for efficient translation of scale.

A relatively new technique for depositing a-Si:H is photo-CVD. Photo-CVD utilizes ultraviolet light to initiate decomposition of silane or disilane. There are several reports of photo-CVD of a-Si:H. These include direct photolysis at 185nm using disilane (2), and mercury sensitized photolysis at 254nm from silane (3) and disilane (4,5). Recently, an 11.2% efficiency a-Si:H p-i-n photovoltaic cell, fabricated by photo-CVD, was reported (6).

The best reported results from both materials properties and device efficiency points of view have been achieved using mercury sensitized photo-CVD. Photo-CVD is the best alternative deposition technique for preparing high quality intrinsic and doped materials, for fabricating devices and for studying fundamental materials/preparation relationships.

Although the reported film quality and device results using the photo-CVD process have been comparable to those of glow discharge, the primary method of preventing deposition on the UV transparent window is to coat it with Fomblin oil which limits the deposition time and makes quantitative analysis of the reactor difficult. In this report we describe a novel photo-CVD reactor which utilizes a moveable Teflon curtain to minimize window fouling. Depositions and characterization of device quality intrinsic and doped a-Si:H layers are described. Finally, the fabrication and analysis of p-i-n solar cells fabricated by photo-CVD are reported.

SECTION 2.0
MATERIAL PREPARATION AND ANALYSIS

Intrinsic and doped (both n- and p-type) hydrogenated amorphous silicon and amorphous silicon-carbide films were grown by ultraviolet photo-CVD using mercury sensitized disilane. While several reactor designs were considered, a novel reactor utilizing a UV transparent moveable Teflon curtain to minimize deposition on the reactor window was designed and constructed. Details of the reactor design, a summary of the film deposition conditions, and characterization of the materials deposited follow in the remainder of Section 2.0.

2.1 PHOTO-CVD SYSTEM, REACTOR AND FILM GROWTH

The evaluation of alternate reactor designs was presented in the semi-annual report under this contract (7). In summary, we felt that none of the existing solutions for preventing deposition on the UV transparent window were entirely satisfactory. We have developed a new photo-CVD reactor with a moveable UV-transparent film and secondary gas flows to eliminate window fouling.

Equipment from the thermal CVD apparatus used in Phase 1 of this contract and additional expenditures by the university were used to build a laboratory for two photo-CVD reacting systems. The gas handling and gas storage was designed for safety and high purity. Key features of the gas manifolds, storage facilities, and reactor construction are described in the semi-annual report(7). A schematic of the photo-CVD reactor is shown in Figure 2-1. As shown in the figure, a flexible curtain separates the reactor into two chambers. In practice, the curtain is mechanically sealed to the walls of the reaction chamber by a weighted plate and dynamically by control of the gas flow rates to minimize diffusion of reactants from the lower to upper chamber.

Reactant and inert gases are fed into the lower deposition chamber after passing over a pool of mercury. The reactant and inert diluent gases are distributed through the reaction chamber by a gas distribution manifold within the reactor.

Inert and/or reaction inhibiting gases are fed into the upper window chamber. These gases can contribute to the reduction or elimination of window fouling in several ways.

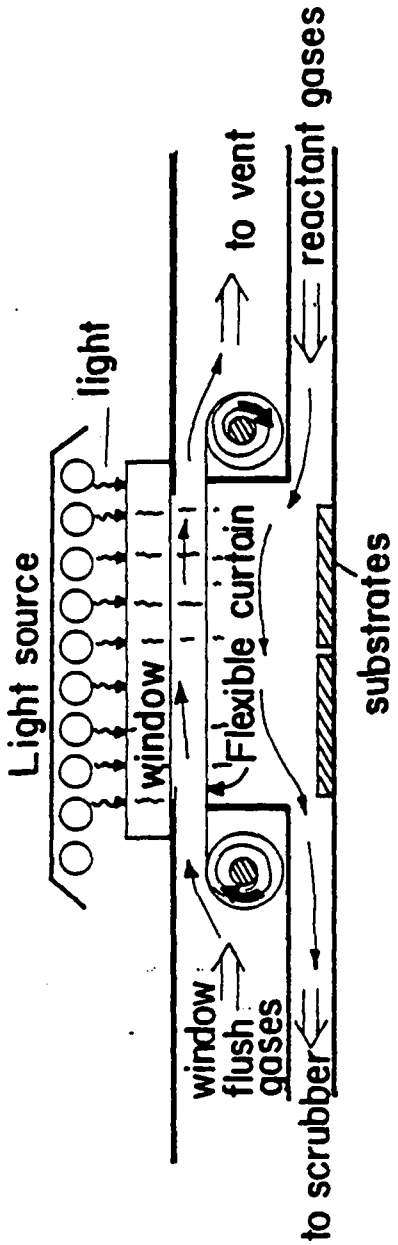

Figure 2-1: Schematic of Institute of Energy Conversion Photo-CVD Reactor

1) Process gases diffusing around the curtain are highly diluted, lowering their partial pressure in the window chamber thus reducing the rate of film growth on the window.

2) Gas phase reactions in the upper chamber can be modified by the gases thus inhibiting formation of the gas phase precursors necessary for film growth.

3) Surface reactions on the window may be modified to minimize film formation.

As described in the semi-annual(7), during the first half of the contract year, the reactor operation was refined to the point where films were successfully deposited without any window fouling. This was accomplished by improvement of the mechanical seal and by using 4%H_{2}/Ar as the window flush. This was not entirely satisfactory since the H_{2}/Ar window flush also resulted in significantly more powder formation in the reaction zone than observed when H_{2}/He was used as the window flush gas. During the second half of the year, a new reactor was built incorporating improved mechanical seals. This reactor operated with essentially no window fouling with any mixture of window flush and reactant gases. Based on the earlier experience the reactor was modified to allow up to 75 linear feet of Teflon film to be loaded. This improvement allows deposition of very thick film or multiple depositions without replacing the curtain. The latter was considered necessary to allow load-locking of the photo-CVD reactor.

As in any low pressure system, the actual substrate temperature and measured substrate holder temperature may be substantially different. Figure 2-2 shows the actual substrate temperature as a function of the measured pedestal temperature at 10 torr operating pressure with flowing He. The temperature difference depends only slightly on the reactor body temperature but does increase at lower pressures. All temperatures reported in the paper are the actual substrate temperature and not the measured substrate holder temperature.

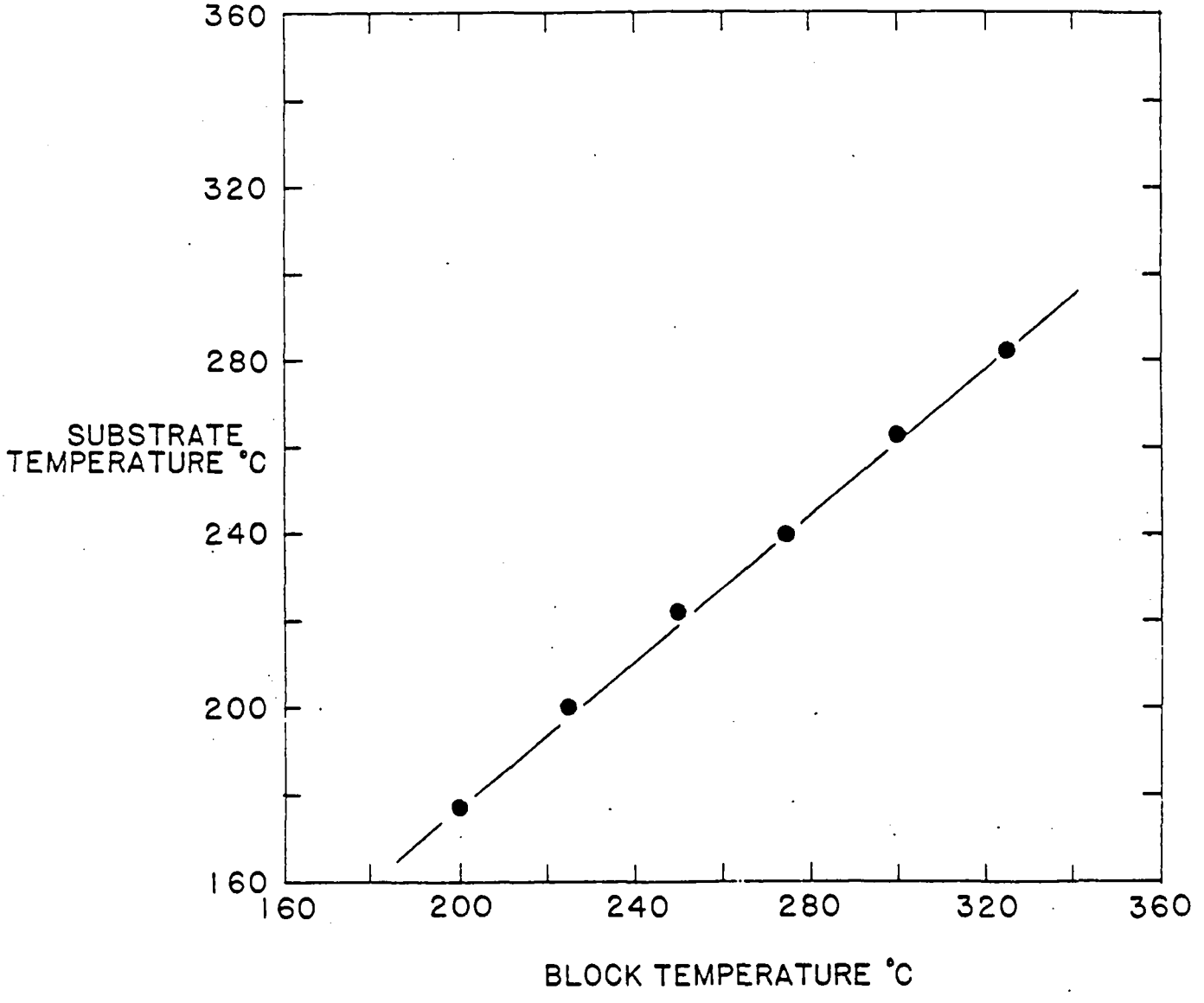

Figure 2-2: Substrate Temperature Calibration with He at 10 torr

The initial intrinsic film depositions reported in the semi-annual were used to develop a preliminary reactor model allowing quantitative evaluation of the effects of film growth on the window and Teflon curtain on the rate of deposition and film thickness(7). The use of this model led to process and reactor design changes which resulted in the growth of intrinsic films over 500nm thick at growth rates around .06 to .07nm/s with no measurable window fouling.

More recently, the model has been extended to also account for the spatially dependent photo-generation of gas-phase film precursors (8,9,10), their diffusion to surfaces inside the reactor, and their subsequent reaction to form films. The model equations consist of component mass balances which account for the diffusion, generation (gas phase reaction or film growth) and depletion (gas phase reaction or film growth) of each species. The model equations and the behavior predicted by the model equations are described below.

The component mass balances for the gas phase, at the substrates, and at the curtain or window are shown in Table 2-1. Also included in Table 2-1 is a balance equation for photons within the reactor accounting for the light attenuation due to absorption by the Hg atoms. Table 2-2 summarizes the reactions which have been included in the species generation and depletion terms. For completeness and future work, the reactions involving GeH_4 and the resulting radicals have been included. The constitutive rate expressions used in the calculations assume all reactions to be first order in each species.

TABLE 2-1: Mass balances used in the photo-CVD model.

- Mass Balances

In gas phase:

$$-\mathcal{D}\frac{d^2 C_i}{dx^2} = G - D$$

where

$\mathcal{D}$ = Diffusion coefficient cm^2/sec
C_i = Concentration of species i in the gas, $\#/cm^3$
G = Generation rate of species, $\#/cm^3/sec$

D = Depletion rate of species, $\#/cm^3/sec$

At substrates:

$$-\mathcal{D}\left.\frac{dC_1}{dx}\right| = k_w\, C_1$$

At curtain (or window)

$$\mathcal{D}\left.\frac{dC_1}{dx}\right| = k_c\, C_1$$

- Light Balances

$$\frac{dI}{dx} = -I\, k_1\, [Hg^o]$$

I = Light intensity @ 254 nm quanta/cm^2/sec
k_1 = Absorption cross section cm^2
$[Hg^o]$ = Concentration of unactivated mercury #/cm^3

TABLE 2-2

Chemical Equations Used in Photo-CVD Model

Deactivation of mercury and generation, G, of radicals

$Hg^* + Si_2H_6 \xrightarrow{k_2} Si_2H_5 + H + Hg^o$ (ref. 10)

$Hg^* + H_2 \xrightarrow{k_3} 2H + Hg^o$ (ref. 10)

$Hg^* + GeH_4 \xrightarrow{k_4} GeH_3 + H + Hg^o$ (ref. 8)

$Hg^* + SiH_4 \xrightarrow{k_5} SiH_3 + H + Hg$ (ref. 7)

Side reactions of stable species with excited H (ref. 8)

$H + Si_2H_6 \xrightarrow{k_6} SiH_3 + SiH_4$

$H + Si_2H_6 \xrightarrow{k_7} SiH_5 + H_2$

$H + SiH_4 \xrightarrow{k_8} SiH_3 + H_2$

$H + GeH_4 \xrightarrow{k_9} GeH_3 + H_2$

Depletion, D, of radicals

$$H + Si_2H_5 \xrightarrow{k_{10}} Si_2H_6$$

$$H + SiH_3 \xrightarrow{k_{11}} SiH_4$$

$$H + GeH_3 \xrightarrow{k_{12}} GeH_4$$

Film formation

$$Si_2H_5 \xrightarrow{k_{13}} \alpha Si{:}H(s)\delta H_2$$

$$SiH_3 \xrightarrow{k_{14}} \alpha Si{:}H(s)+\delta H_2$$

$$GeH_3 \xrightarrow{k_{15}} \alpha Si,Ge{:}H(s)+\delta H_2$$

Figure 2-2 illustrates the calculated film growth behavior of the photo-CVD reactor. The average film growth rate on the substrate depends on the initial growth rate with no curtain fouling (R_{s_0}), the ratio of the growth rate at the curtain to the growth rate at the substrate (γ), and the exposure time of the curtain to the reaction zone. The initial growth rate (R_{s_0}) and the value of γ depend on the Hg partial pressure, reactor geometry, light intensity and spectral content, pressure, temperature, and gas composition and flow rates. Curves 1 and 2 in Figure 2-3 show the average growth rate as a function of curtain exposure time for two initial growth rates (R_{s_0}=1.5 and 6 A/sec) with equal rates of film growth on the curtain and substrate (γ=1.0). At long curtain exposure times the average growth rate is much lower than R_{s_0} due to the fouling of the curtain. At short curtain exposure times the average growth rate nearly equals the initial growth rates indicating much less fouling of the curtain. Curve 3 shows the effect of changing the reaction conditions in a manner which decreases the growth at the curtain relative to that at the substrate (γ=0.25). Operation in this mode yields a higher average growth rate at the substrate. As shown in Figure 2-3, changes in reactor operating conditions which effect R_{s_0} or must be accompanied by appropriate changes in curtain movement to achieve the desired changes. In our experiments, a significant decrease in γ has been observed with the use of silane compared to disilane, with changes in Hg partial pressure, and with decreases in the total pressure and with changes in the curtain to substrate distance. The changes with Hg pressure, total pressure, and curtain to substrate distance are qualitatively consistent with the behavior predicted by the model. The changes occur due to the balance between the spatially dependent light absorption, and diffusion of film precursors to the curtain or substrate. The change in γ with the change to SiH_4 from Si_2H_6 indicates a difference in the chemistry or rates of film growth on the different surfaces. Figure 2-4 illustrates the effect of mercury concentration on the concentration of gas phase film precursors (Si_2H_5 radical) within the reactor. At high mercury concentrations, curve 1, all the available UV light is absorbed by the mercury in the region very close to the curtain. This activated mercury is rapidly quenched by disilane to form Si_2H_5 radicals. Consequently, film precursors are generated preferentially close to the curtain (<0.1 μm away). These radicals must diffuse to the substrate in order to be deposited on the substrates. The higher concentration of radicals at the curtain results in a high growth rate on the curtain further limiting the growth rate at the substrate.

At very low mercury concentrations, curve 3, not all the available UV light is absorbed (~30% for the example shown). As a result, the growth rate at both the substrate and curtain decrease.

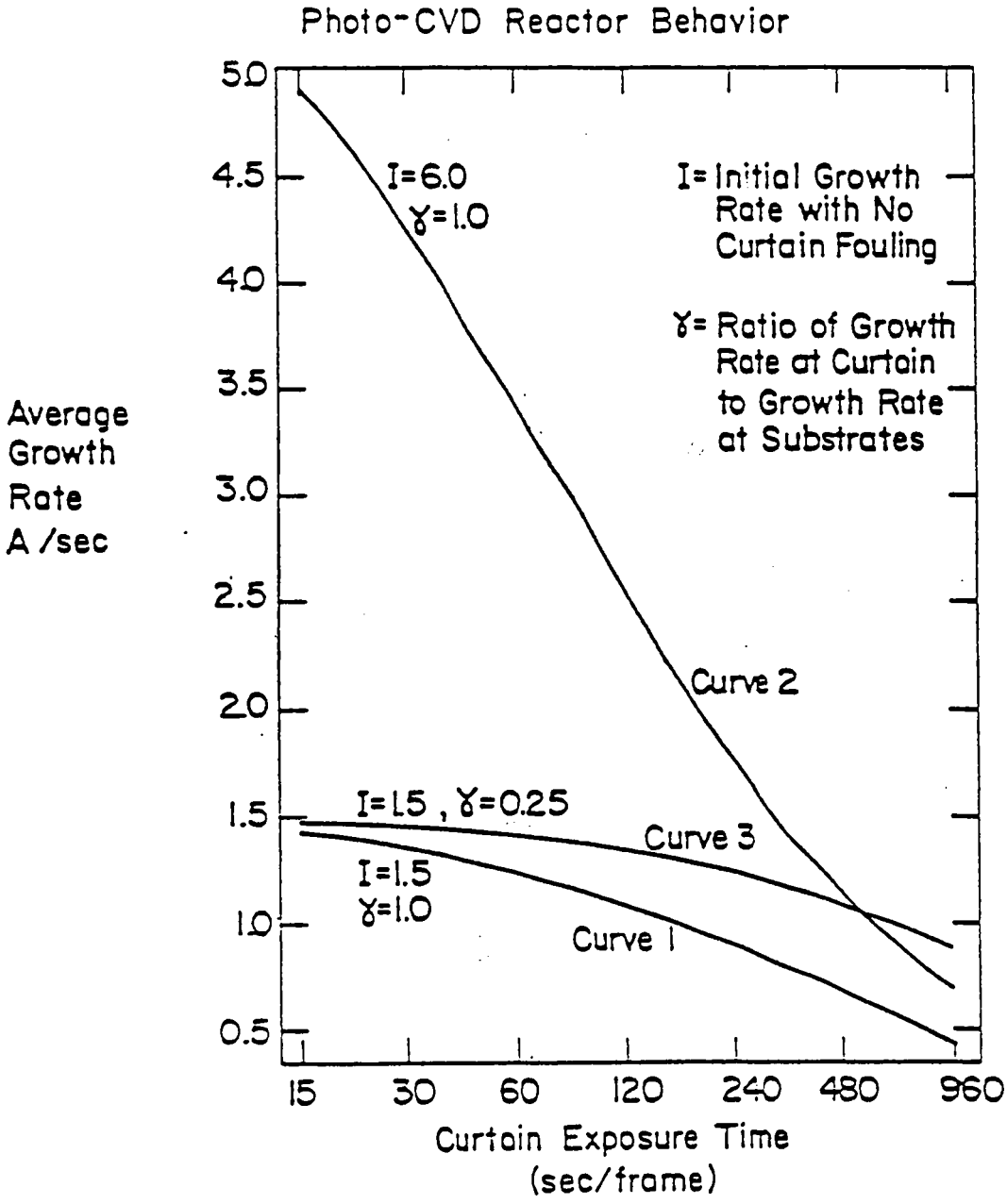

Figure 2-3: Calculated Effect of the Curtain Growth and Exposure Time on the Average Film Growth Rate

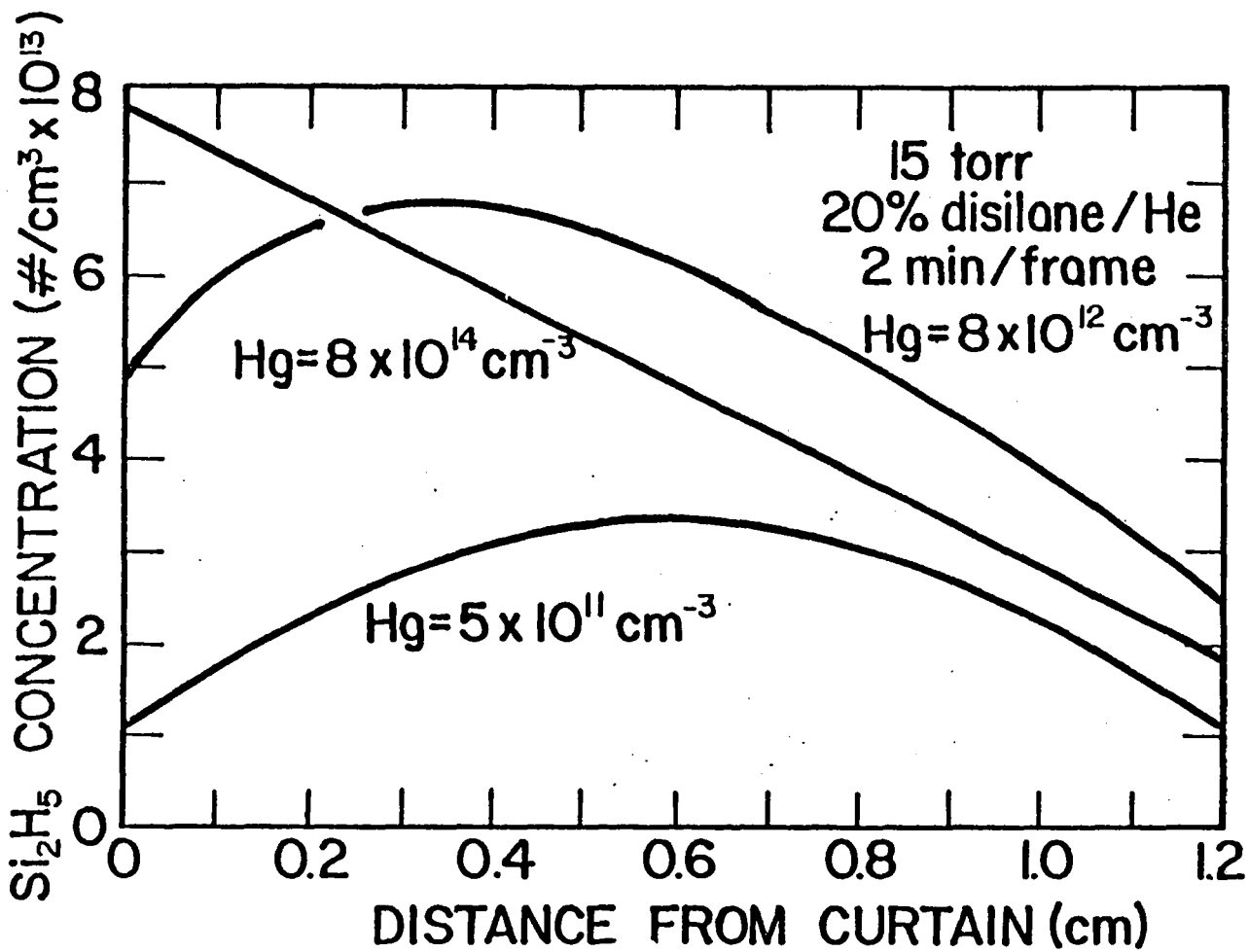

Figure 2-4: Calculated Effect of Hg Concentration on the Si_2H_5 Radical Concentration Profile

For an intermediate (optimum) mercury concentration, curve 2, absorption of the available light and subsequent generation of film precursors occurs throughout the bulk of the reactor. Since more film precursors are formed closer to the substrates, there is less diffusional limitations and a corresponding higher growth rate at the substrates. These model predictions were used to guide modifications to the mercury bubbler and to lower the mercury temperature. As a result the growth rate was nearly doubled.

2.2 Film Characterization

2.2.1 Intrinsic Films

Selected intrinsic layers deposited from silane and disilane at temperatures from 200 to 280°C and pressures of 5 to 15 torr have been characterized using:

1. Optical gap and absorption coefficient.

2. Room temperature dark conductivity and photo-conductivity

3. Dark conductivity as a function of temperature

4. IR absorption spectroscopy

5. Hole diffusion length by surface photovoltage (SPV)

6. Density of states by space charge limited current (SCLC)

7. Sub-band gap absorption from primary photocurrent spectra

Optical absorption coefficients and optical gap were determined from measurements of total reflection and transmission made using a Perkin-Elmer Model 230 spectrophotometer with an integrating sphere. Absorption coefficients as a function of energy were calculated from reflection and transmission data using both the first surface reflection and multiple internal reflection approximations (11). We have found that averaging the intercepts of Tauc plots of absorption coefficients calculated using the front surface and multiple reflection approximations provides a simple and convenient method for estimating optical gap.

The accuracy of intercept averaging to determine optical gap was evaluated by numerical simulation. Arbitrary values of Eg = 1.740 eV and Tauc slope B = 819 $(cm \cdot eV)^{-1/2}$ were used with the Tauc equation to generate "standard" absorption coefficients. The thin film optics equations of Cody et al.(12) in the non-coherent limit were then used to calculate reflection and transmission data. Absorption coefficients were then calculated for comparison to the original "standard" absorption coefficients from the simulated R and T data using the front surface and

multiple internal reflection approximations. Figure 2-5 shows the calculated Tauc plots from simulated R and T data for a 0.5 micron thick film. The average of the intercepts of the first surface reflection and multiple internal reflection Tauc plots is 1.741eV.

Figure 2-6 compares the α obtained by averaging the values obtained from the first surface reflection and multiple internal reflection simplifications to the "standard". The average Tauc plot values are in excellent agreement with the "standard" values; 1.741 eV and B=822 $(cm \cdot eV)^{-1/2}$ compared to 1.740 eV and B=819 $(cm \cdot eV)^{-1/2}$ respectively.

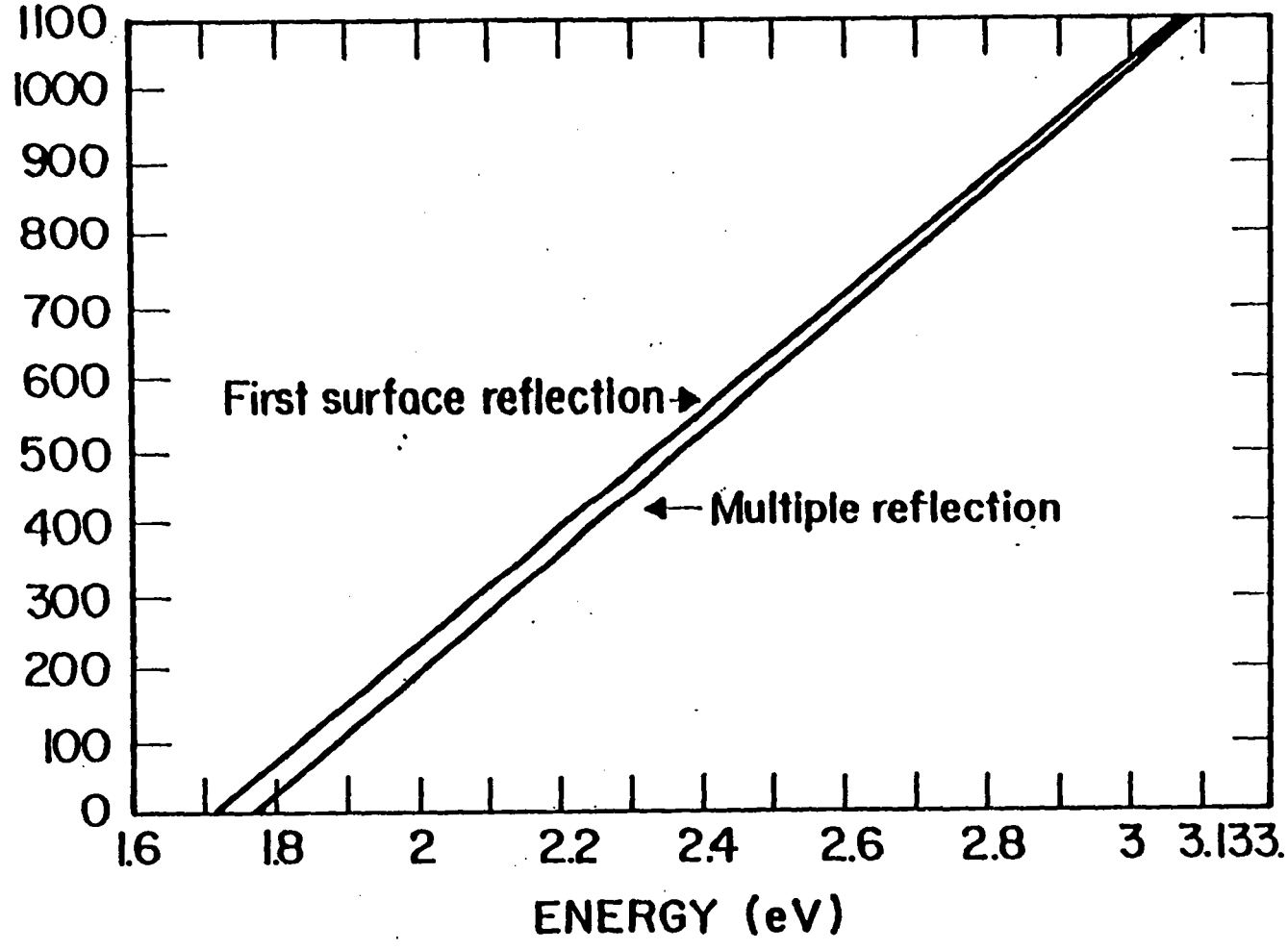

Figure 2-5: Tauc Plot of "standard" Absorption Coefficients Using First Surface and Multiple Internal Reflection Approximation

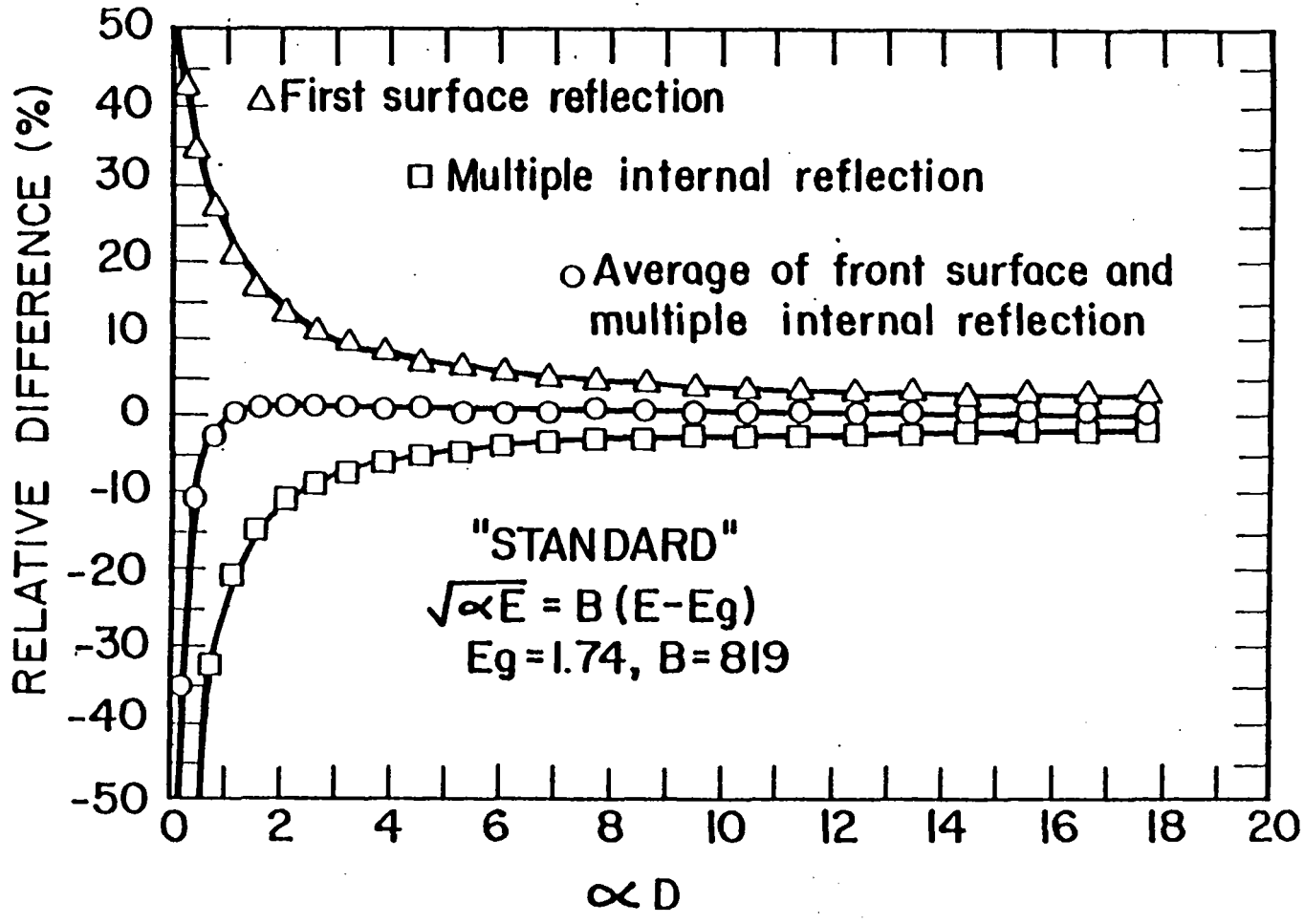

Figure 2-6: Comparison of "standard" Absorption Coefficient to those Calculated from R and T Data Using First Surface and Multiple Internal Reflection Approximations and their Average

Simulations carried out with other film thickness ranging from 0.3 to 1 micron also showed similar agreement between the "standard" optical gap and the average of the front surface and multiple reflection Tauc intercepts. These calculations also indicated that the "average" intercept optical gap is relatively insensitive to errors in film thickness. For example, a 40% error in thickness results in a difference in Eg of only .005eV with a true film thickness of 0.5 μm.

While the optical gap obtained from the Tauc-intercept is a useful benchmark for quick comparison, accurate values of the absorption coefficient are essential for analysis of surface photovoltage and quantum efficiency spectral response data. When $\alpha D<2$, the error in absorption coefficient from either the first surface or the multiple internal reflection approximations exceeds 10%. However, for $\alpha D>0.5$ the "average" absorption coefficient provides sufficient accuracy for analysis of SPV and QE data. Figure 2-6 is a plot of the relative difference between the "standard" and calculated absorption coefficients obtained by applying first surface reflection, multiple internal reflection and average approximations to simulated R and T data.

Figure 2-7 shows typical Tauc plots for a 0.49 micron thick i-layer deposited at 240°C. Values of the optical gap presented in this report are the average of the Tauc intercepts obtained with the front surface and multiple internal reflection approximations.

Dark conductivity as a function of temperature and photoconductivity at room temperature were measured using i-layers deposited on 2000A thick molybdenum contacts 1 mm apart in a gap cell configuration. Photo-conductivity was measured using ELH light at approximately 100 mW/cm^2. Activation energy was determined from Arrhenius plots of $\sigma_d(T)$ measured between 50 and 200°C.

Figure 2-8 summarizes the results of these characterizations for films deposited from disilane at substrate temperatures from 200 to 280°C. Also shown in Figure 2-8 are i-layer film properties reported by Inoue and Konagai(4) deposited at higher flow rates and lower pressures but similar temperatures.

Figure 2-9 presents a comparison of a-Si:H films deposited using both SiH_4 and Si_2H_6. The error bar on the data at 240°C represents the measured range from six separate depositions using disilane.

Room temperature dark conductivity and photo-conductivity have a shallow maximum around 240°C. Typical ratios of σ_p/σ_d are greater than 10^3.

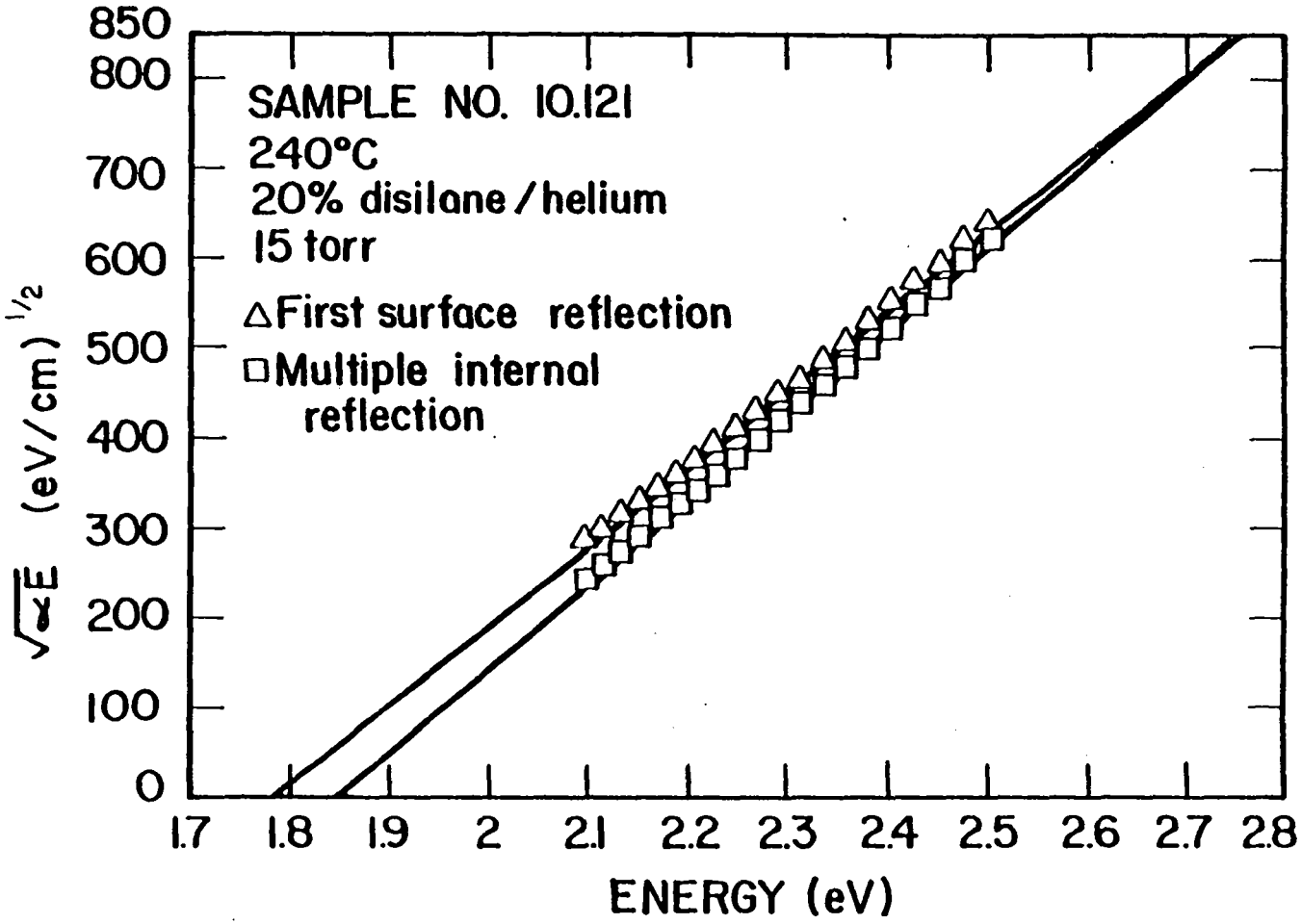

Figure 2-7: Tauc Plot for Typical i-layer (.49 µm thick) Deposited from Disilane by Photo-CVD

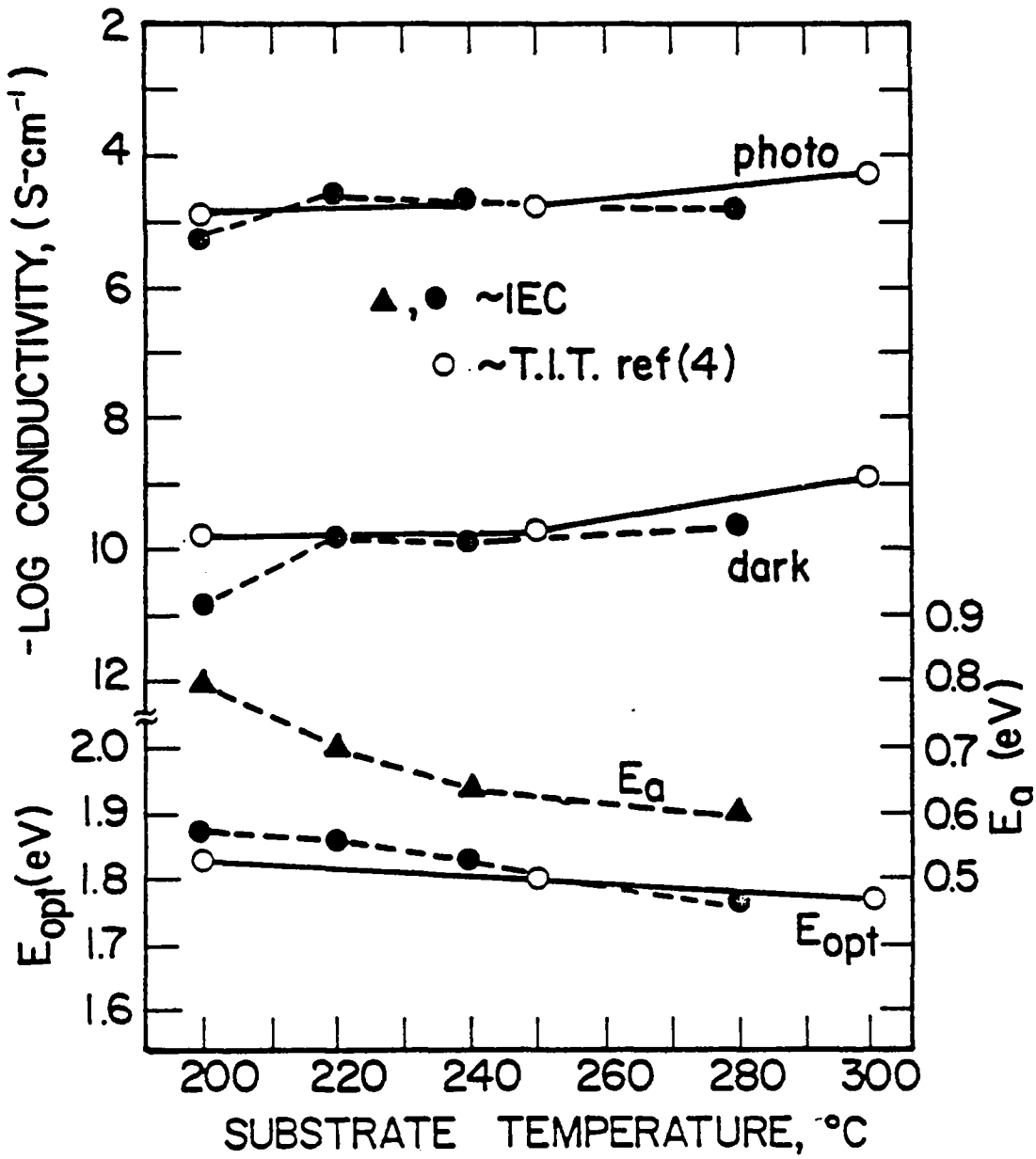

Figure 2-8: Summary of Intrinsic Film Properties Deposited from Disilane

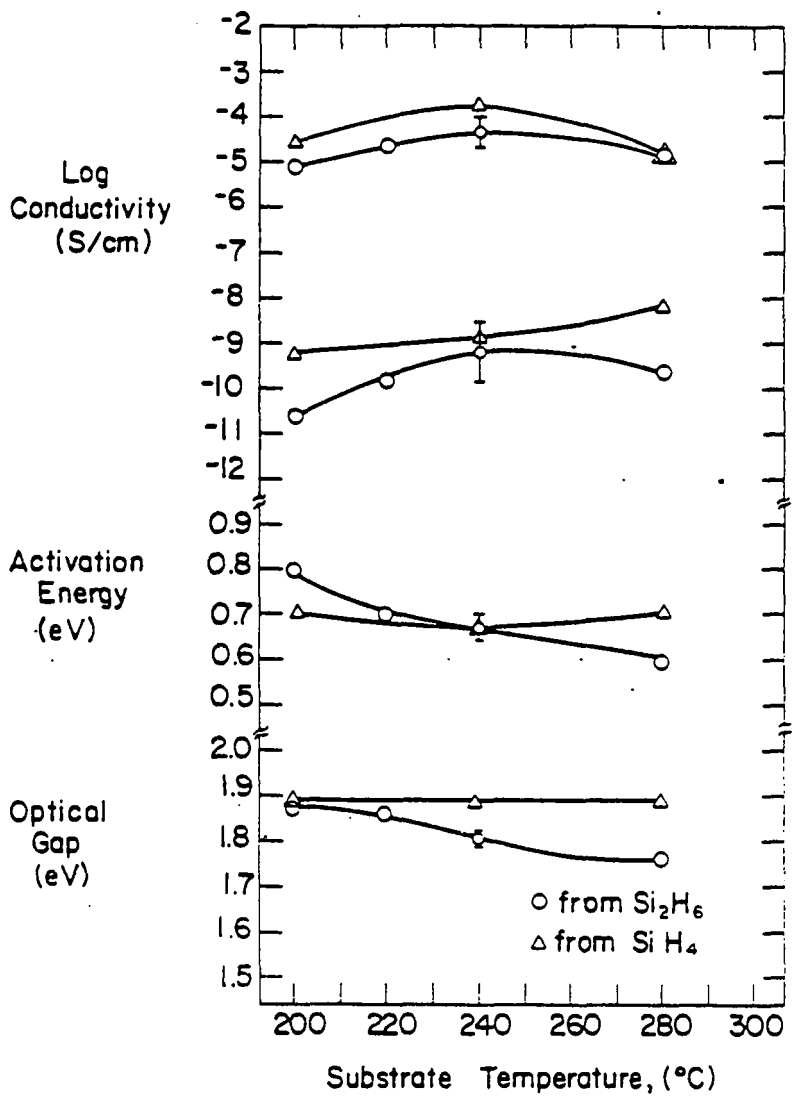

Figure 2-9: Comparison of Intrinsic Film Properties Deposited from Disilane and Silane

IR absorption spectra measured at SERI on samples deposited at 200 and 280°C on single crystal silicon are shown in Figure 2-10. The SiH_2 bond-stretching ($2090cm^{-1}$) and bond-bending ($890cm^{-1}$) is evident in the sample deposited at 200°C while the high temperature sample shows only Si-H bonding. The 630 cm^{-1} absorption peak was integrated to estimate the percent of bonded hydrogen (13) yielding 12% and 6% for the samples at 200 and 280°, respectively.

Very recent results of IR transmission measurements of samples deposited from SiH_4 indicate only Si:H, not SiH_2 bonding at substrate temperatures as low as 210°C. IR measurements on a wider range of samples from SiH_4 will be analyzed to help understand the nearly constant optical gap and dark activation energy over this temperature range.

Diffusion length was measured by the constant surface photovoltage method on intrinsic layers deposited on n^+/Mo/7059 substrates using n^+ by thermal CVD. A value of L_D = .21 μm was obtained with 1 sun red bias light for a .55μm thick i-layer deposited at 280°C as shown in Figure 2-11. The surface photovoltage apparatus has been modified to allow measurement of diffusion length using intrinsic films deposited on 7059/SnO_x substrates (14). Under Phase III thicker films deposited under a wide range of conditions using both SiH_4 and Si_2H_6 will be evaluated.

The density of states (DOS) distribution within the band gap was determined by denBoer's step-by-step method(15) from J-V characteristics measured on Ni/i/n^+(c-Si) sandwich structures. The n^+c-Si wafer was As-doped with a resistivity of .1Ω-cm. The i-layers were approximately .6μ thick. The DOS distributions are shown in Figure 2-12 for i-layers deposited at 240° and 280°C after annealing for 1 hour at 150°C in air. The minimum DOS for the sample deposited at 280°C was approximately twice that of the 240°C sample, $3x10^{16}$ and $1.5x10^{16}$ respectively. The position of the minimum (.63eV) agrees well with the activation energies shown in Figure 2-8. Although these photo-CVD films are less intrinsic than the thermally deposited films (minimum DOS at .63 and .7-.8eV respectively), they have nearly an order of magnitude lower DOS.

In light of recently reported results (16) the DOS measurements will be repeated using much thicker films. In addition, due to difficulty getting good adherence of thick i-layers to previously deposited n+ layers or n-type Si wafers, experiments are underway to use Mg/i/Mg sandwich structures or very narrow gap (2 to 10 micron) Mg or Mo planar configurations for DOS characterization by SCLC.

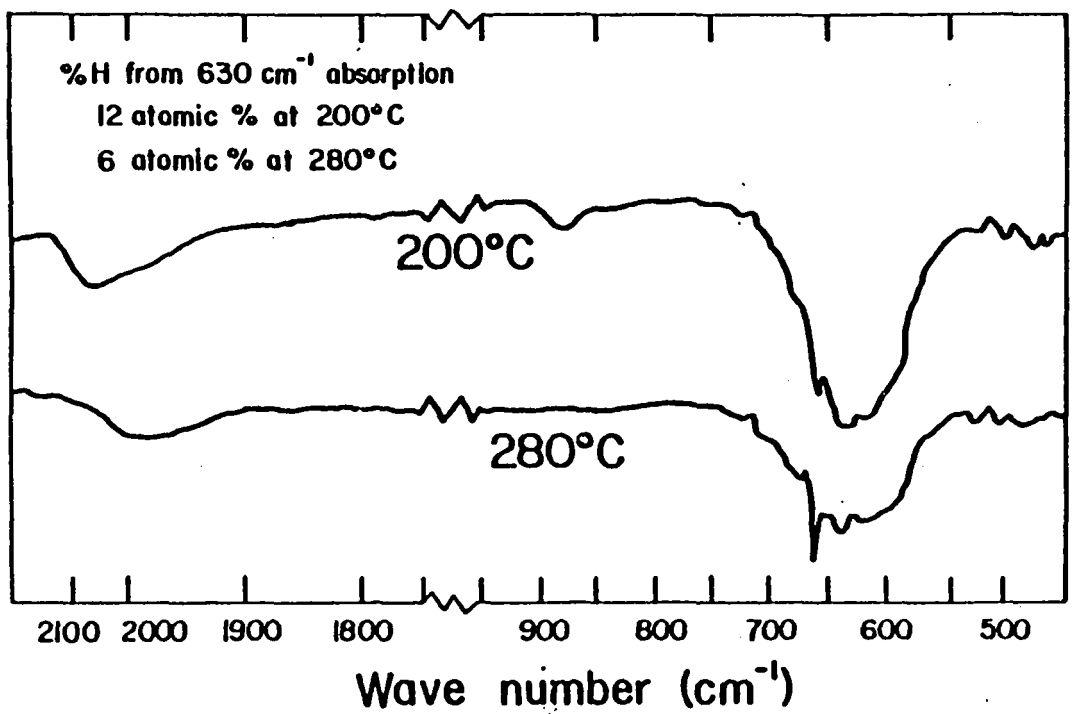

Figure 2-10: Comparison of IR Spectra of Intrinsic Films Deposited at 200° and 280°C From Disilane

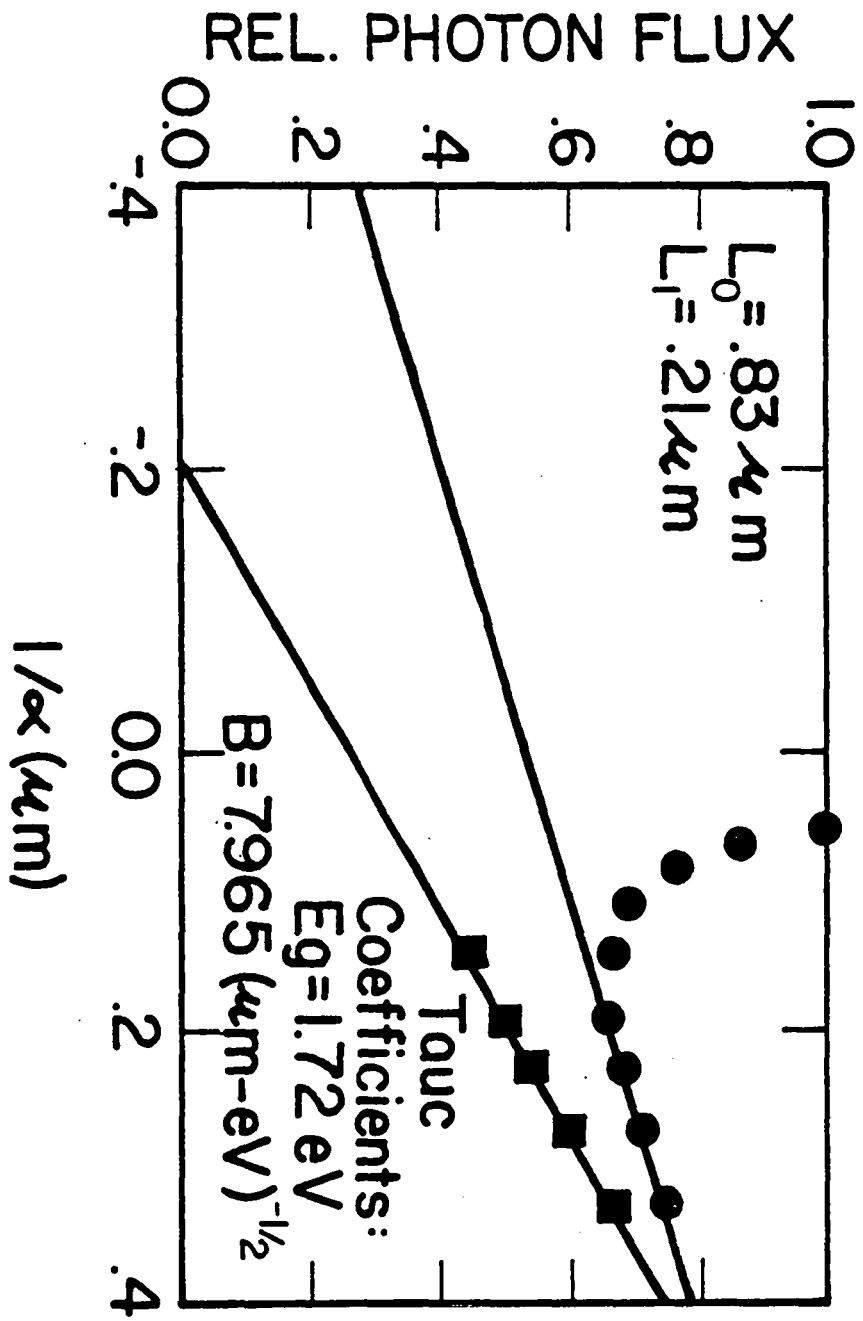

Figure 2-11: Diffusion Length by SPV for Photo-CVD i-layer Deposited on Thermal CVD n-layer

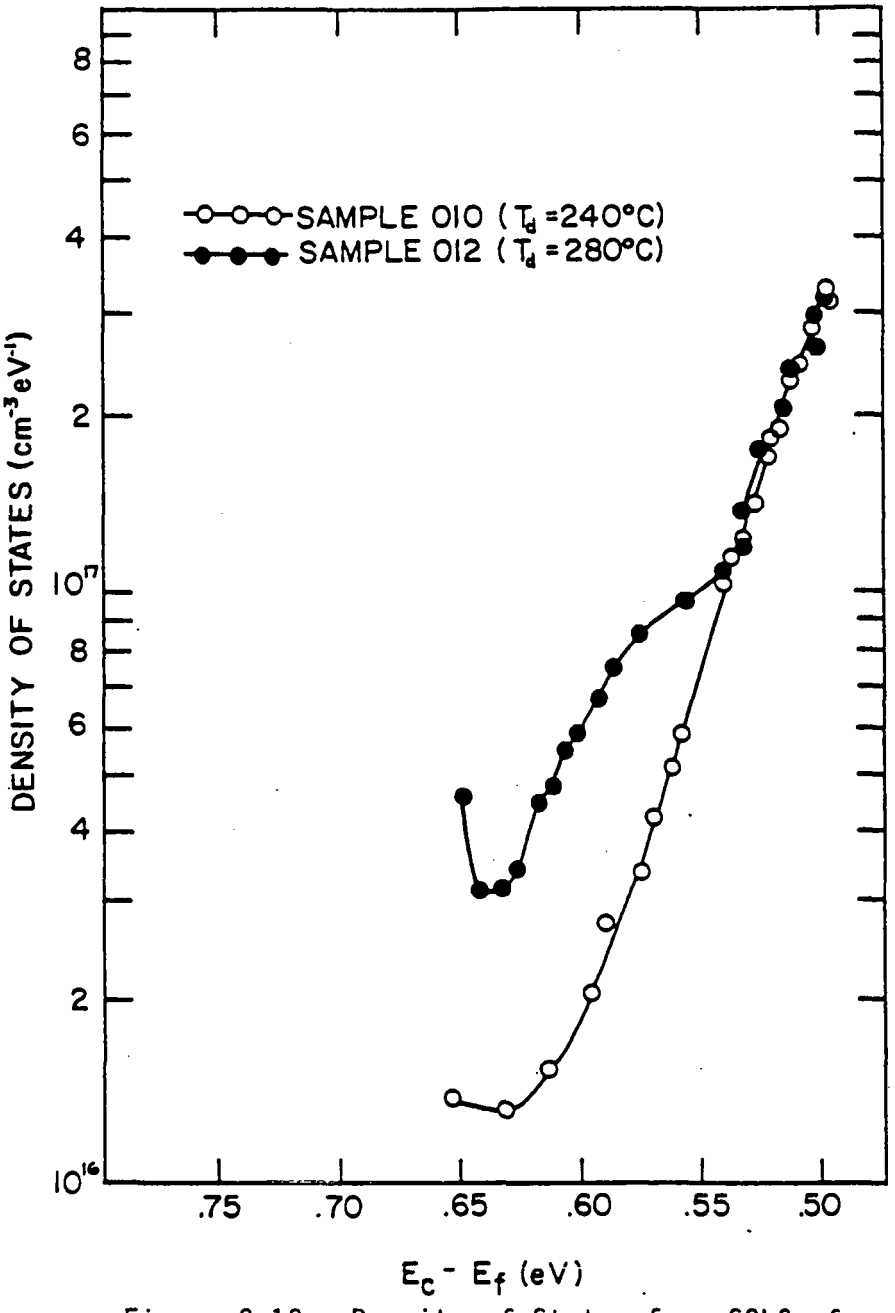

Figure 2-12: Density of States from SCLC of Photo-CVD i-layers Deposited at 240 and 280°C (after 150°C, 1 hr. heat treatment)

The Urbach edge (exponential absorption tail) was determined from the sub-gap primary photocurrent spectra (η_{ac}) shown in Figure 2-13 on a SnO_2/pin/Al device (see Section 3.1). A value of the characteristic energy E_{ch} of .049 eV was obtained from analysis of the slope of ln (η_{ac}) vs E in the range from 1.45 to 1.60eV.

2.2.2 p-layers

The growth and opto-electronic properties of boron-doped p-type a-Si:H films deposited by Hg sensitized photo-CVD using B_2H_6 diluted in He were reported in the semi-annual report(7). The optical gap, room temperature dark conductivity and photo-conductivity and activation energy of the dark conductivity as a function of B_2H_6/Si_2H_6 ratio are summarized in Figure 2-14. Those devices described in section 3 without alloy (a-SiC:H) p-layers were made using p-layers grown with a B_2H_6/Si_2H_6 ratio of 0.013.

More recently, a-SiC:H p-layers have been deposited, characterized, and used in device fabrication. Attempts to use acetylene as the C source resulted in extremely high resistivity films, presumably due to high C incorporation even with a ratio of $C_2H_2/(C_2H_2+Si_2H_6)$ less than 0.1. Better results were obtained using methylsilane and silane.

Figure 2-15 summarizes the opto-electronic properties of p-type a-SiC:H with 10 to 40% methylsilane in silane and a ratio of $B_2H_6/(CH_3SiH_3+SiH_4)$ of 0.015. The conductivity decreases sharply and the optical gap increases from 1.96 to 2.28 eV as CH_3SiH_3 in the feedgas is increased from 20 to 40%. Even at a substrate temperature as low as 165°C there is some evidence of thermal growth especially at the lower CH_3SiH_3 concentration. The best p-layer from this limited number of runs had dark and photoconductivity of $1\text{-}2\times10^{-8}$ S/cm and E_{ch} = 0.38 eV at a bandgap of 1.9 eV. These conditions were used as the starting point for device fabrication (Section 3) although small changes in $B_2H_6/(CH_3SiH_2+SiH_4)$ and $CH_3SiH_3/(CH_3SiH_3+SiH_4)$ have also been explored in the deposition of p-layers in solar cells.

2.2.3 n-layers

Phosphorous doped n-type a-Si:H films have been deposited using Hg sensitized photo-CVD with 10 to 20% SiH_4 or Si_2H_6 in He. Films were deposited using PH_3 in H_2 with PH_3 ratios of 0.01 to 0.02 at a substrate temperature of 240°C. Opto-electronic properties are summarized in Figure 2-14. A doubling in the PH_3 partial pressure and the switch from Si_2H_6 to SiH_4 did not significantly effect the film properties or the pin device performance (Section 3).

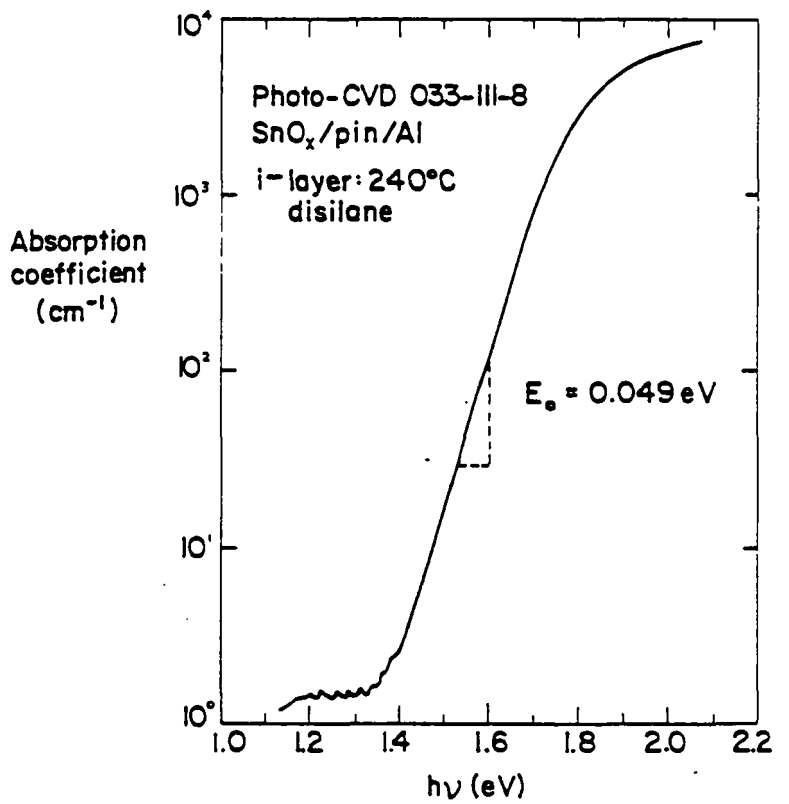

Figure 2-13: Sub-bandgap Absorption from Primary Photo-current Spectrum

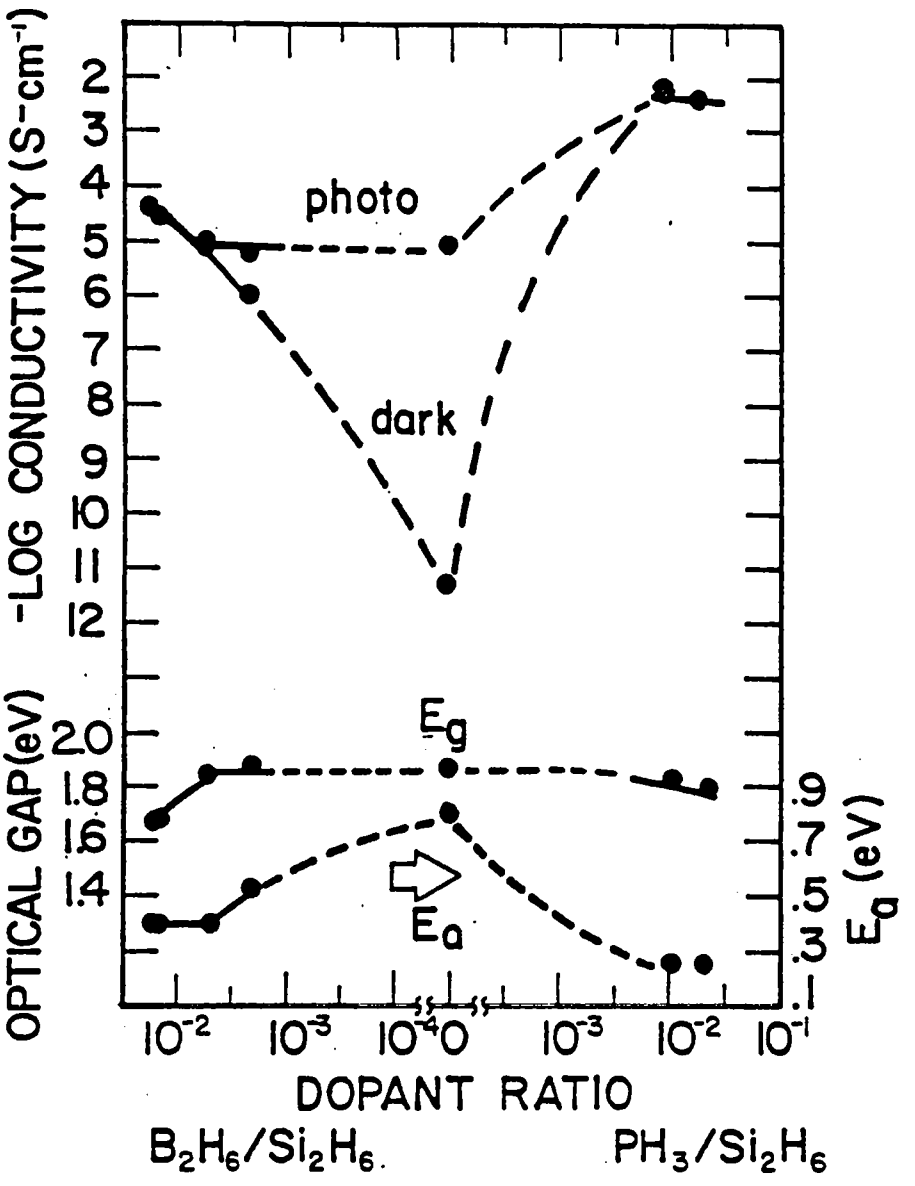

Figure 2-14: Opto-electronic Properties of PH_3 Doped n-type and B_2H_6 Doped p-type Films Deposited by Photo-CVD

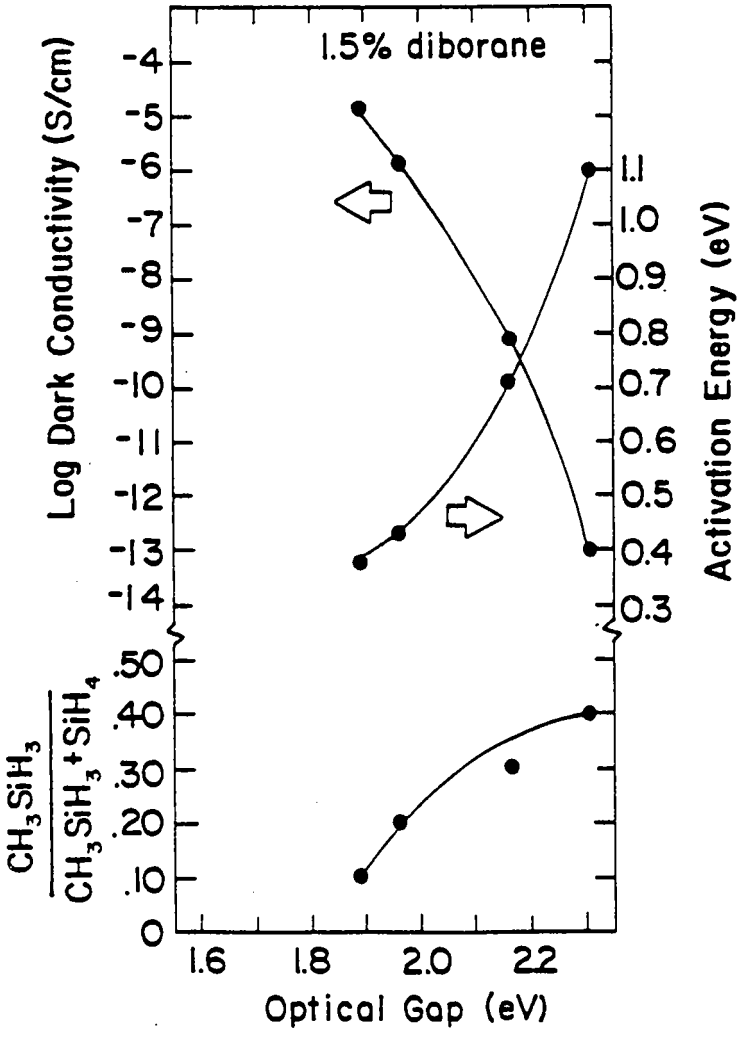

Figure 2-15: Opto-electronic Properties of a-SiC:H Deposited from CH_3SiH_3 and SiH_4

Dark activation energies around 0.25 eV and room temperature dark conductivity between 10^{-9} and 10^{-8} S/cm are typical. The reactor manifolds have recently been modified to allow H_2 dilution during n+ deposition. The effect of H_2 dilution on opto-electronic properties and crystallinity will be studied and reported.

SECTION 3.0
SOLAR CELL FABRICATION AND RESULTS

3.1 Fabrication

Solar cells have been fabricated with doped and intrinsic photo-CVD a-Si:H layers in both system 1 and 2. Most cells have had the structure of glass/TCO/pin/Al although a few doubly-transparent devices with ITO replacing Al have been made for diagnostic purposes. We have used TCO-coated glass substrates obtained from Cherry Display and Nippon Sheet Glass. All results reported here were on devices deposited on Cherry Display SnO_x-coated glass having sheet resistivities of 10-20 Ω-cm.

Both a-Si:H and a-SiC:H boron-doped p-type layers have been used while all n-type layers have been phosphorous doped a-Si:H. As reported in section 2, methyl silane has been used to produce the silicon-carbide layers because of better control of carbon content compared to acetylene.

Intrinsic layer thicknesses of devices ranged from 0.27 to 0.35 μm with 0.30 as typical. Deposition rates were 0.05 to 0.09 nm/sec. During this contract period, most devices were fabricated in system 1 using disilane although some results from system 2 or using SiH_4 are included in this report.

Cell areas of .09 cm^2 were defined using photolithography. Cell testing at IEC was performed with 87.5 mW/cm^2, ELH illumination.

3.2 Results

Devices deposited in system 1 from Si_2H_6 and without silicon carbide p-layers were typically characterized by poor V_{oc} (<.7V), adequate J_{sc} (11-12 mA/cm^2) and good FF (65-69%). We expected to be able to improve J_{sc} with thicker i-layers, enhanced optical reflection from the back contact, and a-SiC:H widegap p-layer as well as improved collection width.

However, the low V_{oc} was puzzling since the barrier height, V_B, determined from measured values of the doped layer activation energies and i-layer bandgap indicated: $qV_B=Eg-E_n-Ep$ = 1.0 to 1.1 eV. This estimate of V_B was verified by analysis of illuminated J(V) characteristics as a function of temperature as described by Han et al.(17). The results are shown in Table 3.1. Simultaneously illuminating and heating backwall samples was not possible and prevented measurements on standard TCO/pin/Al devices, requiring (TCO or Mo)/pin/ITO structures. As seen in Table 3-1, the two structures had very similar V_{oc} values for a given a-Si deposition. Doubly-transparent deposition 063-111 had the same V_{oc} for back or front illumination, indicating that V_{oc} is independent of illumination direction.

TABLE 3-1. Open Circuit Voltage, and Barrier Height for Select photo-CVD pin devices. Method 1 refers to V_{oc} vs T, Method 2 refers to V_{oc} vs J_{sc} vs T as described in reference 17. Experimental difficulties prevented V_b measurements on backwall; illuminated (glass/TCO) cells.

PCVD Substrate	Structure	V_{oc} (V)	V_b (V)	
			Method 1	Method 2
033-111	glass/TCO/pin/Al	0.77	n/a	n/a
033-112	glass/Mo/pin/ITO	0.76	1.27	1.26
034-111	glass/TCO/pin/Al	0.58	n/a	n/a
034-112	glass/Mo/pin/ITO	0.54	0.95	0.90
063-121	glass/TCO/pin/Al	0.68	n/a	n/a
063-111*	glass/TCO/pin/ITO	0.65	1.0	0.97

*V_{oc} was the same for back or front illumination.

From Table 3-1 we reach the following conclusions:

1. Both Method 1 and 2 give comparable values of barrier height.

2. The high V_{oc} for sample 033 is consistent with its larger V_b.

3. Measured V_b agrees well with value calculated from Eg, Ean, Eap.

4. Undesirable reactions with the front (TCO) or back (Al) contacts are not responsible for low V_{oc}. It must be due to problems with the amorphous semiconductor layers.

5. Comparison of these V_{oc} (v_b) values to those predicted by Hack and Shur (Ref. 18, fig. 27) for bulk-recombination-limited V_{oc} indicates that our devices suffer from another loss since a V_{oc} of .72V or greater would be expected for V_b of 1.0V, and a V_{oc}=.88V for a V_b of 1.25V.

Substrate 033.111, which had the highest V_{oc} to date had an initial V_{oc} of around 0.70V which improved to 0.77V following a heat treatment of 175°C in air for one hour. It also had several non-standard process steps, including difficulties controlling gas flow during the p/i transition and n-layer, plasma etching of the a-Si:H layers down to the SnO_x and Ni tabs for contact to SnO_x. Attempts to duplicate the high V_{oc} seen on 033 by duplicating all or part of these steps were unsuccessful.

SIMS data on a typical device (with V_{oc}=0.65V) indicated boron tailing with only slightly better than a two-order of magnitude drop in concentration from the p-layer to the center of the i-layer. We therefore concentrated our efforts on producing a sharp p/i interface to improve V_{oc}. Various process conditions were investigated, including purging with H_2, He or SiH_4 for periods up to 2 hours, several cycles of pressurizing/pumping to dilute the boron, and modifying the reactor to minimize dead space in dopant gas lines. None of these produced open circuit voltages exceeding 0.7V as seen in Table 3-2. We did observe a small improvement (0.09V) as purge time increased from 0 to 30 minutes (compare 058-121 to 059-121 in Table 3-2). It also appears that an overnight pumpdown and bake-out of the Al evaporator improves the FF compared to only an overnight pumpdown.

TABLE 3-2
Typical Device Performance for pin Cells with Variable p-i Purges (all data system 1)

Substrate	Purge	V_{oc}	J_{sc}	FF	n
55.111	10 min He	.64	12.1	67.4	6.0
56.111	10 min He/Si_2H_6	.64	12.0	67.1	5.9
58.121	No purge	.635	11.8	69.2	5.9
60.121	5 min He/Si_2H_6	.645	11.7	68.6	5.9
59.121	30 min He/Si_2H_6	.675	11.9	69.1	6.3

Note: Substrates 55.111, 56.111: overnight pumpdown for Al deposition.

Substrates 58.121, 59.121, 60.121: overnight bakeout for Al deposition.

Tested at 87.5 mW/cm² ELH.

The insensitivity of V_{oc} to these process changes designed to minimize boron contamination of the i-layer may indicate that excess boron is not the first-order problem. High resolution SIMS using an oxygen beam will be used in conjunction with the impurity analysis provided by our RGA to further investigate this problem.

Diode A-factors determined from V_{oc}-ln(J_{sc}) were 1.35±.05, indicating bulk recombination is not a major problem. We are presently involved in a detailed study of the temperature dependence of the "effective" A-factor to determine the diode transport and dominant recombination mechanism. Preliminary results indicate transport is tunnelling-limited. This is consistent with the discrepancy between our measured V_{oc} and that expected based on the measured barrier height since tunnelling dark currents do not 'see' the barrier height potential but instead a much smaller value. Therefore, a much larger dark current results than expected for a given V_b if conventional emission/diffusion over that barrier were governing the transport.

Short circuit currents measured at 87.5 mW/cm² under ELH light have been ranged from 10-12 mA/cm² with the largest value of 12.9 mA/cm². One sample (041-121) was sent to SERI as a deliverable and measured under the Xenon simulator using 100 mW/cm², and corrected to the ASTM-85 global spectrum. Results for cell 7 measured at IEC and SERI are given in Table 3-3, which shows that J_{sc} values measured at IEC are approximately 6 to 7% lower than measured at SERI while efficiency is about 5% higher. This is probably due to differences in spectral content and cell test temperature. IEC is installing an Oriel Xenon global AM1.5 simulator to allow more accurate optimization of cell design.

Quantum efficiency (QE) measurements as a function of voltage bias (19) indicate good collection throughout the device (described in more detail below). Therefore, the main limitation to J_{sc} in our present device design is optical absorption. A wide-gap p-layer, thicker i-layer, and enhanced reflection should improve J_{sc}. The effect of the a-SiC:H p-layer will be discussed later in connection with device results from system 2.

We have investigated the effect of various back contact metals as an alternative to the standard Al. The prime motivation was to obtain enhanced reflection to improve J_{sc}, but potential improvements were anticipated in FF (lower contact resistance) and V_{oc} (reduced barrier oxide layer at the n/metal interface). We selected composite metal layers since past experience showed that Ag films had adhesion problems when deposited sufficiently thick (~1μm) to be mechanically robust, and Mg films oxidize rapidly.

TABLE 3-3. Comparison of IEC and SERI
Cell Test Results for Photo-CVD 141-121-7

Testing Condition	A (cm^2)	T (°C)	V_{oc} (V)	J_{sc} mA/cm^2	FF (%)	n (%)
ELH, 87.5 mW/cm^2 (IEC)	.090	28	.61	11.7	67.0	5.5
Xenon, ASTM Global (SERI)	.089	25	.62	12.5	66.0	5.2

Metal contacts were electron-beam deposited on one substrate each from Run 060 (5 minute p/i purge) and Run 062 (30 minute p/i purge) with approximate thicknesses as follows: Al(1μm); Ag/Al(.01/1μm); Mg/Al(.01/1μm); Ag/Mg/Al(.01/.01/1μm). The results of J-V measurements before and after heat-treatment are shown in Table 3-4.

There was no trend of Voc with contact metal. Cells from 062 always had higher Voc than those from 060, consistent with the small improvement due to a longer purge as just discussed. Surprisingly, Ag/Al reduced J_{sc} while Ag/Mg/Al increased J_{sc}, compared to Al. Quantum efficiency measurements clearly showed this behavior to be caused by changes in collection beyond 600 nm. consistent with improved generation due to reflected light.

The efficiency improved slightly for all substrates with a heat-treatment of 1 hour at 150°C in air, primarily due to a 2-3% increase (absolute) in FF. The best photo-CVD cell efficiency to date was 060-122-3 with Ag/Mg/Al contact which has V_{oc}=.644V, J_{sc}=12.9 mA/cm^2, FF=67.9%, and n=6.44% after heat treatment. The J-V behavior of this cell is shown in Figure 3-1.

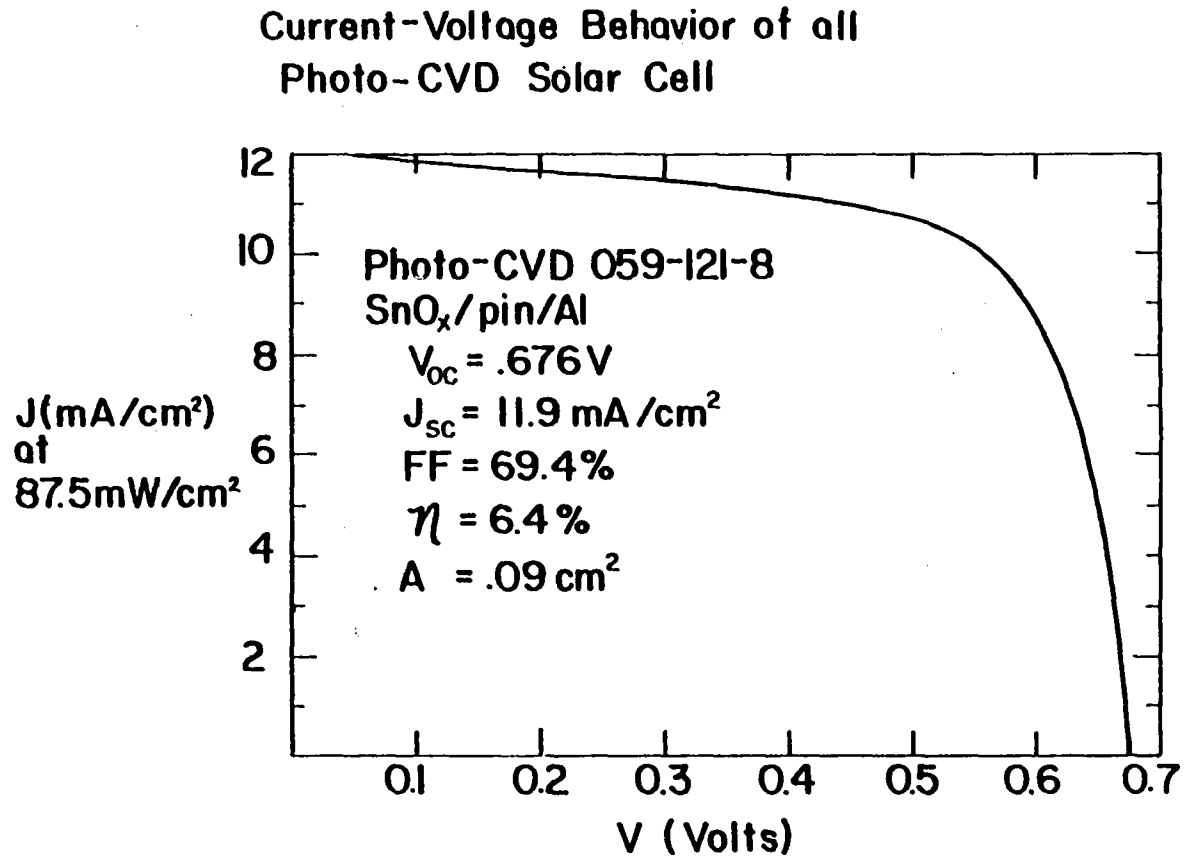

Figure 3-1: Current-Voltage Behavior of Best All Photo-CVD Solar Cell

TABLE 3-4: Effects of back metal contact and heat treatment (1 hour, 150°C, air) on J-V characteristics of highest efficiency cell from each substrate. (B=Before H.T., A=After H.T.)

PCVD Substrate		Back Metal	V_{oc} (V)	J_{sc} (mA/cm²)	FF (%)	N (%)
060-121	(B)	Al	.642	12.2	64.7	5.81
	(A)		.648	11.7	69.2	6.02
062-121	(B)	Al	.675	11.4	65.9	5.78
	(A)		.680	10.9	67.8	5.72
060-111	(B)	Ag/Al	.627	10.7	66.8	5.13
	(A)		.628	11.2	68.2	5.48
062-111	(B)	Ag/Al	.638	10.2	66.8	4.95
	(A)		.646	10.3	68.5	5.21
060-112	(B)	Mg/Al	.640	11.8	65.5	5.65
	(A)		.645	12.1	68.2	6.07
062-112	(B)	Mg/Al	.634	10.9	64.4	5.10
	(A)		.647	11.1	68.2	5.61
060-122	(B)	Ag/Mg/Al	.642	12.9	65.5	6.18
	(A)		.644	12.9	67.9	6.44
062-122	(B)	Ag/Mg/Al	.677	11.8	65.0	5.95
	(A)		.682	11.9	66.6	6.17

Devices with only Al showed a small decrease in J_{sc} with heat treatment while the others showed small increases or no change, indicating Al migration may be occurring (a reasonable assumption at 150°C) but this can be blocked by the second metal layer which acts as a diffusion barrier. Since there was little difference in J_{sc} before heat treatment between devices receiving Al and those with Mg/Al or Ag/Mg/Al we decided to continue using Al for our standard metallization. We may use a different back contact when optimizing cell performance for high efficiency later in the program.

Quantum efficiency measurements as a function of light and voltage bias have been made on a large number of samples. Changes in the QE between light and dark gives information relating to the photo-hole trapping effect to the field profile while voltage bias dependence can indicate limiting carrier, interface recombination and other effects(17).

Figures 3-2 and 3-3 show the QE of 033-111-4 before and after heat treatment, including scans at 0V bias with ELH. Note that the 0V light and dark scans are nearly identical, while reverse bias increases the response more in the blue after heat treatment than before. Figure 3-4 shows the QE for the short circuit case (0V,ELH bias) of this cell before and after heat treatment of 1 hour at 175°C in air, which caused J_{sc} to decrease from 10.2 to 8.9 mA/cm^2 while V_{oc} increased from 0.7 to 0.77V. It indicates that the source of these changes with heat treatment is associated with the p/i interface or electron collection width. Both of these effects are related to electron recombination, not holes which usually governs QE.

Figure 3-5 shows the QE of 059-121-3 before heat treatment. Note that there is a large difference between the 0V light and dark scan while the voltage bias dependence is very small, and independent of wavelength. After heat treatment, the V_{oc} remained unchanged (.66V) and J_{sc} decreased only slightly (12.3 to 12.1 mA/cm^2). This cell behavior is typical of most devices deposited in system 1 and in direct contrast to the results from 033-111-4 (Figures 2-15, 3-1, 3-2).

The lack of significant voltage bias dependence of the QE in Figure 3-5 together with the relatively high FF (68%) indicates that there is negligible collection losses due to electron or hole recombination and the hole collection width is greater than the i-layer thickness (typically 0.3 μm). This implies that both the interfaces and the i-layer are of sufficient quality that they are not the prime efficiency limitations. This conflicts with the conjecture that the p/i interface contamination is responsible for low V_{oc}. Poor p/i interfaces, such as due to boron tailing, are clearly identified by the large bias dependence of QE at short wavelengths (19). However, it is possible that the electric field at interface is so large that it

masks the excess electron recombination by sweeping the electrons away from p/i interface before they recombine.

The series resistance has been analyzed using the Swartz method (20) where $R_{V_{oc}}$ is measured as a function of intensity. This allows the various contributions to $R_{V_{oc}}$ to be identified as $R_{V_{oc}}=R_c+R_L+R_D$, where R_c is the contact (light-independent) resistance, R_L is the photoconductive resistance (of the i-layer) and R_D is the diode resistance (AkT/qJ_L). Results from 4 cells are shown in Table 3-5. These values are typical of those reported for high efficiency glow discharge devices, and indicate that series resistance is not a major loss factor in FF. For example, 039 and 041 had identical $R_{V_{oc}}$ but significant differences in FF.

Devices from system 2 have typically had similar J_{sc}, slightly higher V_{oc}, and poorer FF compared to devices whose results have been reported above from system 1. This is unexpected due to the presence of the wide-gap a-Si:C:H which should improve V_{oc} substantially and J_{sc} slightly. We have been able to achieve V_{oc} exceeding 0.7V only with combination of the wide-gap p-layer and a 1 hour turbo pump purge cycle between the p and i-layers. We have produced cells in system 2 with disilane and silane, with a-Si:H and a-Si:C:H p-layers, with various purge, pump-down, and bake-out cycles, yet V_{oc} has not exceeded 0.73V. The possible effect of O contamination from air or H_2O is presently being investigated using a residual gas analyzer and SIMS analysis. Recent SIMS analysis made on p-i-n devices in both systems 1 and 2 indicate slightly higher oxygen and nitrogen in the films deposited in system 2. Unfortunately, the relatively few measurements made are not conclusive due to variation from sample to sample and to large differences (15X) on different SIMS machines. The investigation of impurity incorporation is continuing.

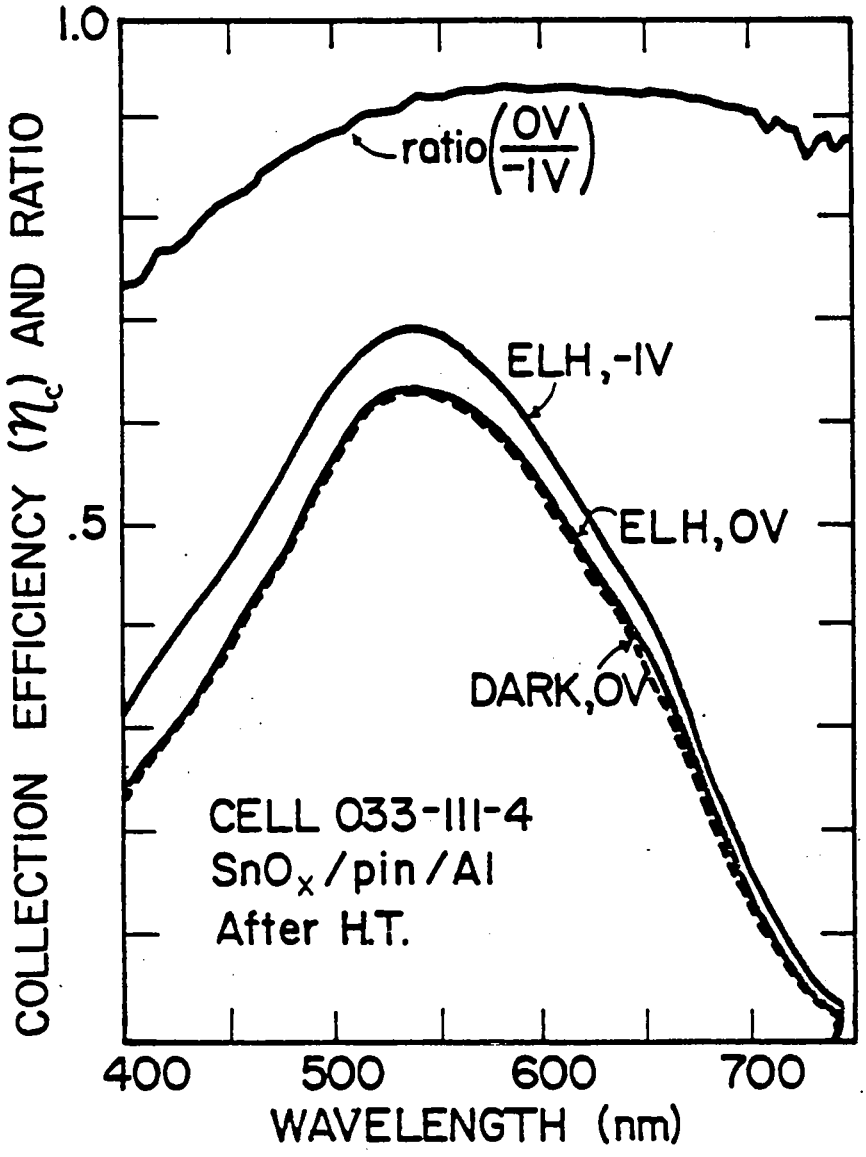

Figure 3-2: Effect of Voltage and Light Bias on Collection Efficiency for Cell 033-111-4 Before Heat Treatment

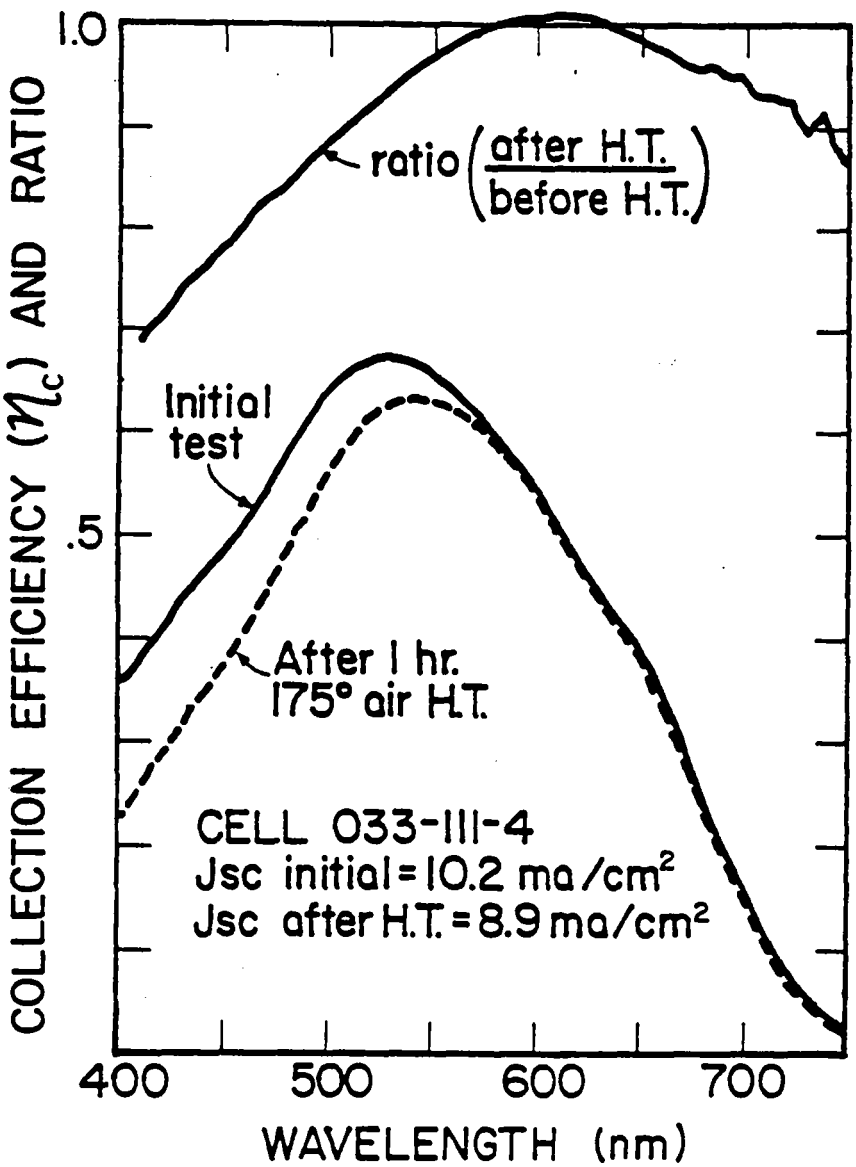

Figure 3-3: Effect of Voltage and Light Bias on Collection Efficiency for Cell 033-111-4 After Heat Treatment

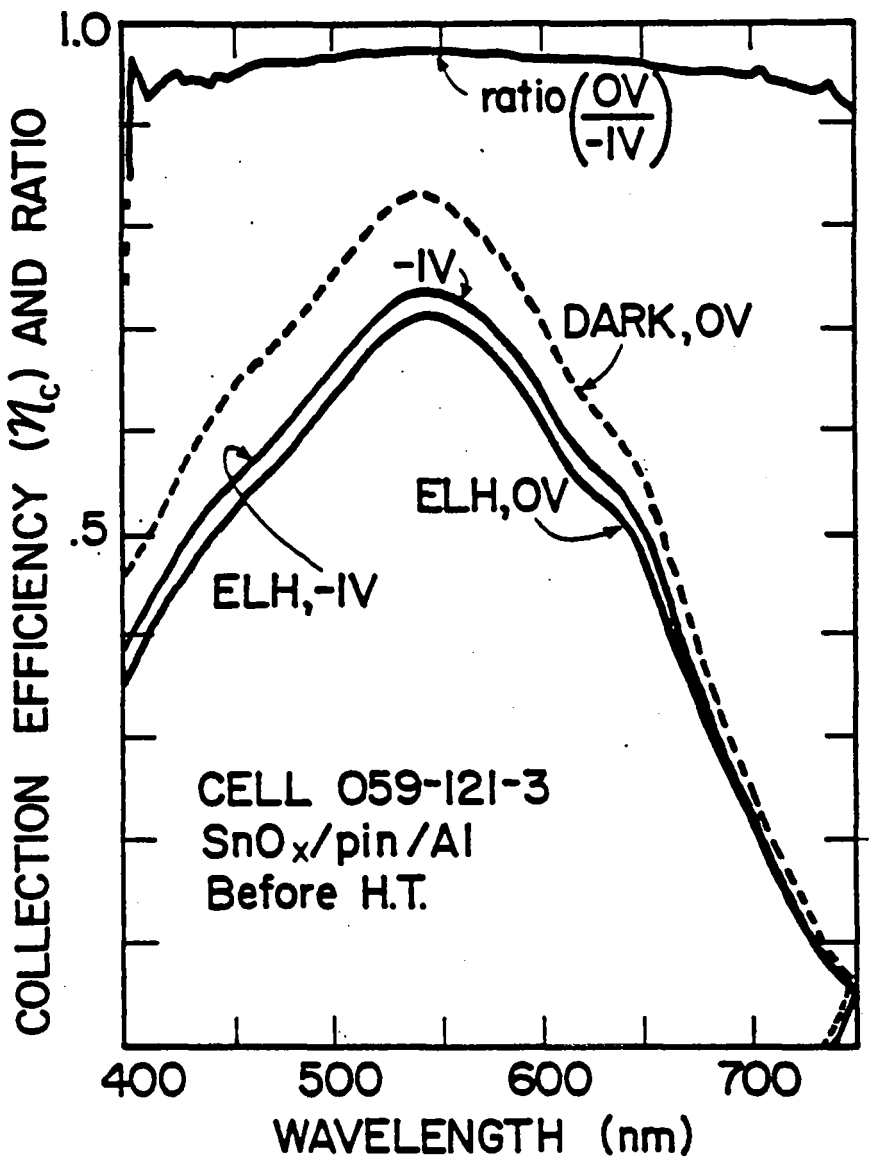

Figure 3-4: Comparison of Collection Efficiency for Cell 033-111-4 Before and After Heat Treatment under ELH Bias Light

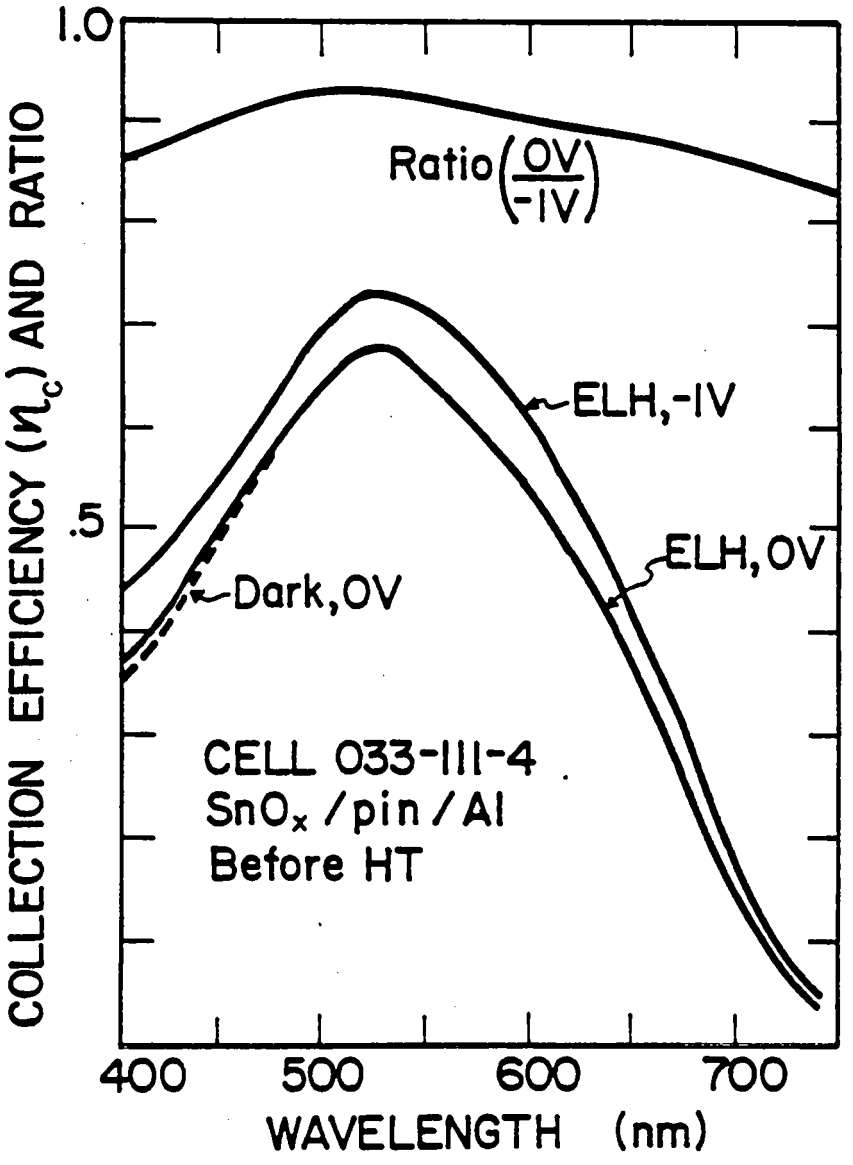

Figure 3-5: Effect of Voltage and Light Bias on Collection Efficiency for Cell 059-121-3 Before Heat Treatment

TABLE 3-5. Series Resistance Analysis of R_{vcc} Using Swartz Method (R_{vcc} measured at 87.5 mW/cm², R_G, R_L, R_D calculated from intensity dependence).

PCVD	FF (%)	R_{vcc}	R_G (in ohm-cm²)	R_L	R_D
033-111-5	64.6	6.86	1.0	1.9	4.5
034-121-10	65.0	5.34	1.1	1.3	3.0
039-122-12	63.9	5.21	0.80	1.5	3.1
041-111-4	69.3	5.36	0.74	1.3	3.4

SECTION 4.0

REFERENCES

1. R. E. Rocheleau et al. in Materials Issues in Applications of Amorphous Silicon Technology. MRS Symposia Proceedings Vol. 49. pp 15-20.

2. Y. Mishima et al. Japan J. Appl. Phys. 22, L46(1983).

3. T. Saitoh et al., Appl. Phys. Lett. 42(8), 678(1983).

4. T. Inoue et al., Appl. Phys. Lett 43(8), 774(1983).

5. A. E. Delahoy et al. in Materials Issues in Applications of Amorphous Silicon Technology. MRS Symposia Proceedings Vol. 49. pp 33.

6. M. Konagai to be published in Materials Issues in Applications of Amorphous Silicon Technology. MRS Symposium Proceedings of Symposium E, April 14-18, 1986 Palo Alto, CA.

7. B. N. Baron, R. E. Rocheleau, S. S. Hegedus, "Photochemical Vapor Deposition of Amorphous Silicon Photovoltaic Devices", SERI/STR-211-2967, Golden, CO, Solar Energy Research Institute (1986).

8. Y. Rousseau and G. J. Mains, J. of Phys. Chem., 70, (10), Oct 1966, pp. 3158-3162.

9. H. Niki and G. J. Mains, J. of Phys. Chem., 68, (2), Feb. 1964, pp. 304-309.

10. T. L. Pollock, H. S. Sandhu, A. Jodhan, and O. P. Strausz, J. of the American Chem. Soc., 95 (4), Feb. 21, 1973, pp. 1017-1024.

11. J. L. Pankove, Optical Processes in Semiconductors, Prentice-Hall, Englewood Cliffs, NJ 1971 pp 93-95.

12. G. D. Cody et al., Solar Cells 2(3), 227 (1980).

13. H. Shanks et al., phys. stat. sol.(b)100, 43(1980).

14. A. R. Moore and H. S. Lin, submitted to J. Appl. Phys.

15. W. den Boer, J. Phys. C4, 451(1981).

16. I. Solomon, R. Benferhat, and H. Tran-Qyec,Phys. Rev. B 30, 1984.

17. M. Han, P. Sung, W. Anderson, Electron Dev. Lett. 3, 121, (1982).

18. M. Hack, M. Shur, J. Appl. Phys. 58, 997, (1985).

19. V. Dalal, M. Leonard, J. Booker, A. Vaseashta, S. Hegedus, Proc. 18th IEEE Photovoltaic Conf., 837, (1985).

20. G. Swartz, Semiconductors and Semimetals, Vol. 21D, J. Pankove, Ed., Academic Press, 39, (1984).

Document Control Page	1. SERI Report No. SERI/STR-211-3114	2. NTIS Accession No.	3. Recipient's Accession No.

4. Title and Subtitle
Photochemical Vapor Deposition of Amorphous Silicon Photovoltaic Devices, Annual Subcontract Report, 1 May 1985 - 30 April 1986

5. Publication Date
February 1987

6.

7. Author(s)
B. N. Baron, R. E. Rocheleau, S. S. Hegedus

8. Performing Organization Rept. No.

9. Performing Organization Name and Address
Institute of Energy Conversion
University of Delaware
Newark, DE 19716

10. Project/Task/Work Unit No.
3493.10

11. Contract (C) or Grant (G) No.
(C) XB-4-04061-1
(G)

12. Sponsoring Organization Name and Address
Solar Energy Research Institute
A Division of Midwest Research Institute
1617 Cole Boulevard
Golden, Colorado 80401-3393

13. Type of Report & Period Covered
Technical Report

14.

15. Supplementary Notes
Technical Monitor: Byron Stafford

16. Abstract (Limit: 200 words)
Intrinsic, p-type, and n-type a-Si:H and p-type a-SiC:H thin-films have been deposited by Hg-sensitized photochemical vapor depositions (photo-CVD) from disilane. The photochemical reactor design includes two chambers separated by a movable UV-transparent Teflon curtain, which eliminates deposition on the reactor window. Photovoltaic devices of the type glass/TCO/p-i-n/metal were fabricated by photo-CVD. The device efficiency obtained at 87.5 mW/cm^2 and ELH illumination was 6.4%.

17. Document Analysis
a. Descriptors Amorphous state ; silicon solar cells ; thin films ; chemical vapor deposition

b. Identifiers/Open-Ended Terms

c. UC Categories
63

18. Availability Statement
National Technical Information Service
U.S. Department of Commerce
5285 Port Royal Road
Springfield, Virginia 22161

19. No. of Pages
56

20. Price
A04

Form No. 0069 (3-25-82)